Finite Element Model of Hydro Generators Coupled to a Grid Simulation Software

PAR

Gilles ROSSELET

acceptée sur proposition du jury:

Prof. A. Rufer, président du jury
Prof. J.-J. Simond, Dr M. Tu Xuan, directeurs de thèse
Dr S. Keller, rapporteur
Prof. J. R. Mosig, rapporteur
Prof. M. M. Radulescu, rapporteur

ÉCOLE POLYTECHNIQUE
FÉDÉRALE DE LAUSANNE

Suisse
2010

Remerciements

Par ces quelques lignes, je tiens à remercier tous les collègues, parents ou amis et membres du jury qui par leurs encouragements, soutien et conseils m'ont aidé à mener ce projet à son terme.

Avant tout, j'aimerais faire part de ma reconnaissance au Professeur Jean-Jacques Simond. J'aimerais le remercier de la confiance qu'il m'a témoignée en me permettant de faire ce travail de doctorat au sein du LME, ainsi que pour la grande liberté qu'il m'a accordée tout au long de ce travail.

J'aimerais également remercier le Dr Mai TuXuan dont l'expertise et les précieux conseils m'ont permis de mener à bien cette entreprise.

Je remercie les membres du jury qui ont aimablement accepté de consacrer du temps à l'analyse du manuscrit de ma thèse, le Prof Alfred Rufer, le Prof. Mircea Radulescu, le Prof. Juan Mosig et le Dr Stefan Keller.

Il me faut aussi remercier, pour le soutien financier qu'ils ont apporté à ce projet: la firme ALSTOM power et l'Office Fédérale de l'Energie.

Je remercie mes amis et collègues de LME pour l'extraordinaire ambiance de travail qu'ils ont su créer.

Sur un plan plus personnel, j'aimerais remercier mes parents dont les encouragements et le soutien m'ont permis de faire des études.

Que chacun trouve ici l'expression de ma profonde gratitude.

Résumé

La simulation de systèmes d'énergie électrique (entraînements à vitesse variable, éoliennes, réseaux complets, . . .) utilise le modèle de Kirchhoff. Il s'ensuit que chacun des composants du système ainsi simulé (ligne de transmission, disjoncteur, machines électriques) est représenté par un circuit équivalent.

Ces circuits équivalents sont incapables de prendre en compte précisément les effets non-linéaires dont les machines électriques sont le siège.

Ces effets (courants de Foucault, saturation magnétique, effet pelliculaire) sont néanmoins prédits avec précision par la méthode des éléments finis.

Le but de cette thèse est d'ajouter à un logiciel de simulation de systèmes d'énergie électrique (appelé dans ce texte simulateur de réseaux) un modèle éléments finis d'une machine électrique particulière, l'hydro-générateur.

Cette thèse examine tout d'abord la nature du lien entre un simulateur de réseau et le modèle éléments finis. Ensuite un logiciel de calcul par éléments finis, destiné uniquement à simuler des hydro-générateurs et à être lié avec un simulateur de réseaux, est développé.

IV

Les caractéristiques que doit avoir un tel programme sont imposées par la physique du dispositif à modéliser. Il s'agit de la capacité de gérer la saturation magnétique des matériaux, de prédire les courants de Foucault et de gérer les mouvements du rotor de la machine. De plus, ce programme doit permettre d'utiliser les symétries du dispositif étudié pour réduire le temps de calcul ainsi que la mémoire nécessaire à sa simulation.

Ces caractéristiques sont validées individuellement, avant d'être utilisées ensemble pour simuler un hydro-générateur.

Mots-clé:

FEM, méthode des éléments finis, calcul numérique de champ, machine électrique, courants de Foucault, saturation magnétique, bande de roulement, simulation couplée

Abstract

For the simulation of electrical power systems (adjustable speed drives, wind farms, complete grids, etc.) the Kirchhoff's model is used. Each of the components of this model (transmission line, circuit breaker, electrical machines, etc.) is represented by an equivalent circuit.

These equivalent circuit models are unable to take precisely into account the non-linearities of the electrical machines.

These non-linearities (eddy currents, magnetic saturation of the materials, skin effect) are however accurately predicted by the finite element method.

The goal of this thesis is to add a finite element model of an electrical machine, the hydro generator, to a grid solver.

The nature of the link between the grid solver and the finite element model is first investigated. Then, a finite element program used solely to the simulation of the hydro generator and to its link with a grid solver is designed.

The features required for such a program are mandated by the physic of the device modelled: dealing with non-linear materials, eddy currents and taking the movement of the rotor into account.

Furthermore, it is possible to use the symmetries of the studied device to reduce both the calculating time and the necessary memory.

All these features were validated individually, before being used together in the simulation of a hydro generator.

List of the variables

Scalars

A	[Wb/m]	Component of the vector potential along the z axis	p19
A_i	[Wb/m]	Value of the vector potential on node i	p20
b_v	[m]	Width of the cooling ducts	p10
h	[m]	Equivalent length of the FE model	p10
h_a	[m]	Actual length of the sheet-metal stack	p10
H	[A/m]	Magnetic field	p22
i	[A]	Current	p22
I	[kg· m^2]	Moment of inertia	p69
i_b	[A]	Squirrel cage, current between two neighbouring bars, bottom	p89
i_c	[A]	Current on the circuit side	p31
i_{fem}	[A]	Current on the FE side	p31
i_f	[A]	Field current	p68
i_t	[A]	Squirrel cage, current between two neighbouring bars, top	p89
J	[A/m^2]	Component of the current density along the z axis	p19
k	[-]	Binary boundary condition, linking factor	p73
k_{em}	[N·m]	Electromagnetic torque	p69
k_{ext}	[N·m]	External torque	p69

VIII

Scalars cont.

Scalars cont.

u_v	[V]	Squirrel cage, total voltage	
		on a bar and the switch in series with it	p89
V	[V]	Electric potential	p18
z_v	[-]	Number of cooling ducts	p10
α	[rad]	Angular position of the rotor	p30
α_i	[-]	Shape function on the node i	p20
δ_0	[m]	Minimal width of the air-gap	p10
ε	[F/m]	Permittivity	p18
ε	[A]	Coupling error	p31
μ	[H/m]	Permeability	p18
ρ_q	[C/m^3]	Free charge density	p18
σ	[1/(Ω·m)]	Conductivity	p25
Φ	[Wb]	Flux in a single turn	p22
ψ	[Wb]	Total flux	p22
ω	[1/s]	Angular frequency	p43

X

Vectors and matrix

$\mathbf{A}$	[Wb/m]	Vector potential	p18
$\mathbf{B}$	[T]	Flux density	p18
$\mathbf{C}$	[m/(V·A)]	FE induced current matrix	p26
$\mathbf{D}$	[1/Ω]	Jacobian matrix of the coupling error	p33
$\mathbf{E}$	[V/m]	Electrical field	p18
$\mathbf{J}$	[A/m^2]	Current density	p18
$\mathbf{K}$	[A·m/V]	FE differential matrix	p25
$\mathbf{M}$	[A·m/Wb]	FE algebraic matrix	p22
$\mathbf{N}$	[-]	FE source matrix for uniform current density region	p22
$\mathbf{S}$	[1/Ω]	FE source matrix for eddy currents region	p25
$\mathbf{T}$	[m]	FE induced voltages matrix	p24

Contents

1

Introduction

The study of the behaviour of an electric grid or a variable speed drive usually uses Kirchhoff's model. This kind of model is based on the notion of circuit and the associated equations. Each component in a topology (transmission line, transformers, circuit breaker...) is represented by an equivalent circuit.

The electromagnetic transducers in general, and the rotating machines in particular, exhibit non-linear phenomena (saturation of the magnetic circuit, eddy currents...), which cannot be taken into account accurately by Kirchhoff's models. A precise prediction of these phenomena can however be obtained by a finite elements (FE) model of the machines.

The FE method is based on the actual geometry of the studied device. At each time step it computes the flux density on all points of the geometry. This, in turn, enables the accurate computation of the saturation, eddy currents and skin effect.

The goal of this work is to replace the equivalent circuit model of the synchronous machine by a FE model in SIMSEN, a grid solver developed at the LME since 1990.

At the beginning of this work, the exact nature of the link between the FE model and the grid solver was unknown. So as not

to limit the choice in this matter, it was desirable to have access to the source code of the FE program. This of course ruled out using a commercially available program. Two solutions remained: The first one was to rewrite a new FE program dedicated only to the simulation of synchronous machines and to the link with SIMSEN. The other was to use one of the programs available under a free license and adapt it for these two tasks. As it was difficult to assess beforehand the time gained by this solution, it was decided to write a new program from scratch.

For reasons that are made clear in (sect. 2.1), the machines considered for this work are laminated rotor salient pole generators with damper cage. The requirements for a FE program able to simulate such a machine are:

- ability to deal with non linear materials;
- ability to take eddy currents into account;
- slide-band;
- simulation of a fraction only of the machine by taking its symmetries into account;
- ability to be linked to a grid simulation program e.g., SIMSEN;
- computing speed for future industrial use.

This thesis is organized as follow: The chapter 2 lists the requirements for the FE program to be written. The necessary theory is dealt with in (ch. 3). This chapter first briefly introduces the field equations that are solved by the FE method, then describes the chosen linking method and concludes with a remark on the time solver used.

The chapters 4 to 6 contain each an application validating one of the necessary feature of the program.

The chapter 4 presents the simulation of a single-phase transformer. It provides a first check of the ability to deal with non-linear material and the link with a grid solver. Two massive conductors are then added to the transformer to validate the prediction of eddy currents.

The chapter 5 describes the simulation of a three-phases transformer. This simulation provides a further check of the link with an external grid solver.

The slide-band and the simulation of a fraction only of the machine are demonstrated in (ch. 6), by the simulation of a simple synchronous machine.

The chapter 7 checks the implementation of the damper cage by simulating an induction machine and (ch. 8) presents the simulation of a synchronous machine. Each of these applications has been validated by comparison with Flux2D. Finally (ch. 9) provides a general conclusion.

1.1 Literature overview

The topic of circuit–field coupling is a subset of the multiphysic simulation, so named because they mandate the simultaneous resolution of equations arising from different physical phenomenon. A comprehensive list of different coupled problems of interest in the domain of electrical machines is given in [1].

The majority of the literature published on the field-circuit coupling deals with one of the following methods:

- direct coupling;
- lumped components;
- current or voltages output approach.

These three methods will be briefly described and a selection of relevant and current publications will be provided.

The direct method is the most straightforward of the three. The coupling is simply dealt with by concatenating the circuit and FE equations in the same system. They are then solved together by a single solver. Application examples are given in [2] and [3], while [4] describes a method to assemble the circuit equations such so that resulting system remains symmetrical.

With the lumped component model, the device modeled with the FE method is represented in the circuit solver by a set of inductances, resistances and voltage sources, whose values are updated by the FE solver. The advantage is obvious as very few, if any, changes are necessary to the circuit solver.

The computation of the value of the equivalent lumped components is dealt with in [5], [6] and [7]. The two latter articles also provide application examples: The simulation of a permanent magnet generator for [6] and the prediction of the currents in the damper cage and pole shoes of a turbo generator for [7]. Further applications are available in [8] and [9].

The current output approach considers the FE model as a set of voltage dependent current sources, the other way round for the voltage output approach. The values of the sources are updated at the end of each time step according to the current or voltages previously computed.

The implementation of this method is discussed in [10] using MATLAB as circuit solver. Application examples are given in [11], [12], [13] and [14].

In this work a method allowing to treat the link as the resolution of a non-linear equations set is introduced. It is adapted from the method presented in [15]. This method is further developed in [16].

Commercial circuit and FE programs increasingly offer facilities to link them to each other. The circuit and system solver Simplorer [17] have been successfully linked to iMoose [18] in [6], Flux2D [11] and Maxwell2D [19], [13].

The latest version of Flux2D from CEDRAT can be linked to both Portunus [20], a simulator of mechatronic systems, and the well-known MATLAB.

The design of a simulation software using equivalent circuit model is detailed in [21]. An example of mixed analytic-circuit model is given in [22].

2

Requirements for the FE software

This chapter is divided in three sections. First, a short description of the machines considered in this work is provided. Then, the modelization of electrical machines by the FE method is shortly described. After that, based on these descriptions the requirements themselves are drawn. Finally, the chapters in which each of the requirements are further discussed are listed.

2.1 Machine structure

The hydro generators are synchronous machines coupled to hydro turbines, hence their name. Their main common characteristics include:

- short axial length but large diameter (up to 18 [m], Three Gorges' Dam machines)
- salient pole rotor
- star-connected stator winding
- usually a low speed with a consequently large amount of poles, from 4 up to 100
- complete or partial damper cage

- laminated stator and rotor

Their poles shoes are either made of a single piece of forged steel, or by a stack of electromagnetic iron sheets. Each sheet being isolated from the other. From a simulation point of view their main difference is that the forged ones allow the circulation of eddy currents, whereas the stacked ones do not. For this work, only the machines with a laminated rotor and a damper cage will be considered.

2.2 General characteristics of the model

2.2.1 Basic notions

The basic notions of the FE and the relevant vocabulary is defined here. The FE method enables to solve partial differential equations, the Maxwell equations in the case at hand. This method is based on a discretization of the plane by a set of non-overlapping triangles, the mesh (2.1). Each triangle is an element. The elements are defined by their vertices, the 'nodes' of the mesh.
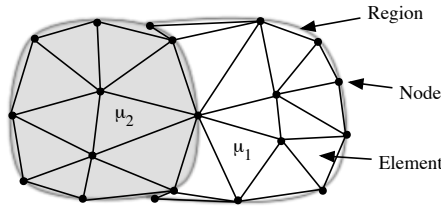

Fig. 2.1. Mesh example.

Each of the different parts of a machine (windings, stator and rotor yoke, damper bars, etc.) are modelled by one or several regions. A

region is a surface on which the physical characteristics (permeability, magnetic characteristics, etc.) are uniform. The nodes, regions and the segments defining their borders are collectively called the geometry of the problem.

2.2.2 Mesh

The shape and size of the elements in the mesh have a direct influence on the quality of the simulations. The FE method is made in such a way that the approximation it delivers converges to the real solution when the size of the elements gets to 0. It is therefore reasonable to wish to build a mesh with as many and as small elements as possible, keeping in mind that each additional variable uses memory and slows the solving process.

The shape of the elements also plays a role. The best approximation is obtained when the elements shape is as close as possible to an equilateral triangle. Needle-shaped elements, who have one or two angles much smaller than the others, are to be avoided.

To sum up, a good mesh has small elements where the flux density varies quickly and bigger elements were it is almost uniform. For example in (fig. 2.2) the air gap, pole shoe as well as the teeth of the stator have been finely meshed, whereas the center of the rotor yoke has bigger elements. It is particularly important to finely mesh the damper bars, in order to accurately predict the currents they carry (c.f. [23] p2.8).

2.2.3 2D FE model

Because of the complex shape of the electrical machines (fig. 2.3) it would be logical to use a 3D model. However simulations with such a model needs a prohibitively long running time. To overcome this problem a 2D FE model of the active part of the machine is used. The impedance of the end winding and the short-circuit ring of the damper cage are taken into account by adding resistor and inductor to the accompanying circuit.
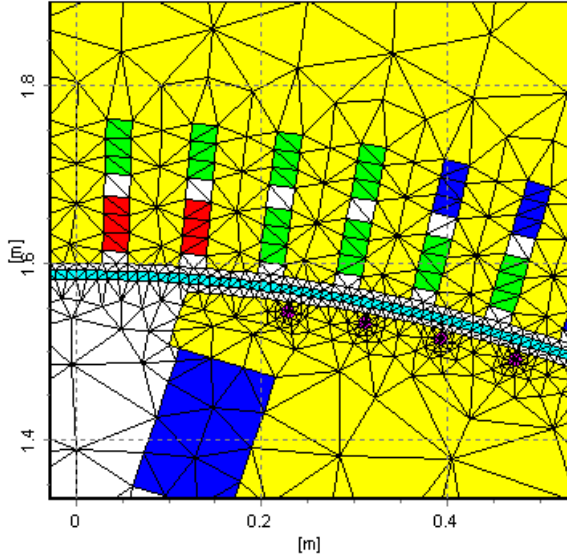
Fig. 2.2. Typical mesh of a salient pole machine.

The 2D FE model along with the added component is known as a 2.5D model. It enables a very good prediction of the transient behaviour of the machine without the complexity of a full 3D model.

The conditions under which a 2D model can be use are listed in [24] p239, namely:

1. the size of the geometry is long along one axis, compared to that of its cross section;
2. the cross sections are identical along this axis;
3. the flux lines can be assumed to be perpendicular to the axis;

Even if the first condition is not satisfied by the hydro generators, they are nevertheless successfully modelled in 2 dimensions. See [23] for examples of transient simulations.
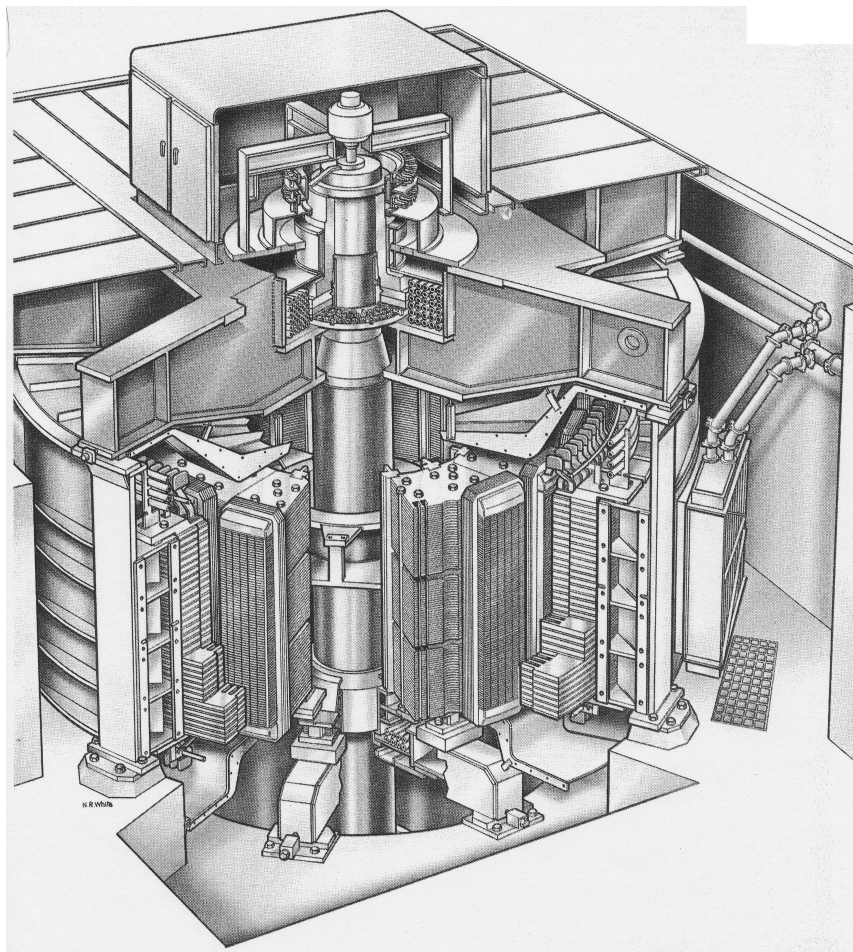
Fig. 2.3. Cross cut of a hydro generator.

For the computation of flux, it is assumed that the active part has an equivalent height of h (fig. 2.4). This height is not the actual size of the lamination as the cooling ducts reduced the surface available for the flux to flow through. The formula (2.1) for the computation of h is established in [23] p2.24.

$$h = h_a - z_v \frac{b_v^2}{5\delta_0 + b_v} \qquad (2.1)$$

Where h_a is the active length of the machine (i.e. the actual length of the stack of iron sheets), z_b the number of cooling ducts, b_v their width and δ_0 the minimal width of the air gap.
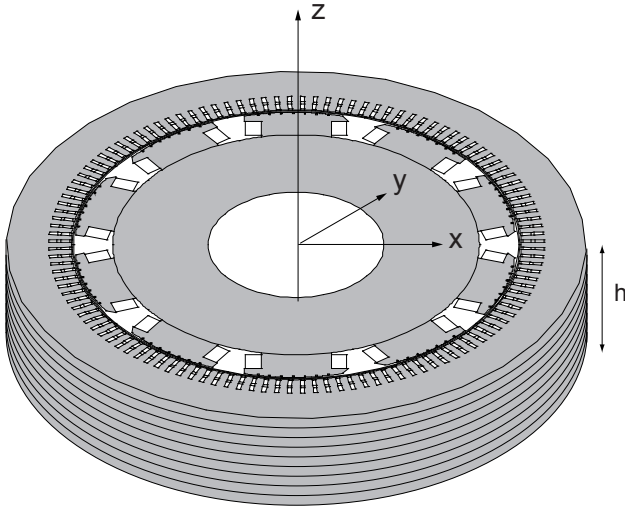

Fig. 2.4. Stator and rotor iron.

2.2.4 Periodic and anti-periodic boundary conditions

Two types of boundary conditions are needed. First homogeneous Dirichlet condition is used to create borders through which no flux can pass. This condition is applied to the outer border of the stator and the inner border of the rotor as no flux is supposed to leave the machine nor flows through the shaft.

Periodic and anti-periodic boundary conditions are then used to reduce the computing cost of the simulation. The idea is to simulate only one period of the machine, which significantly reduces the size of the needed mesh. The figure 2.5(a) shows a typical geometry for a hydro generator. The fraction that will be used for the FE modelling is highlighted.
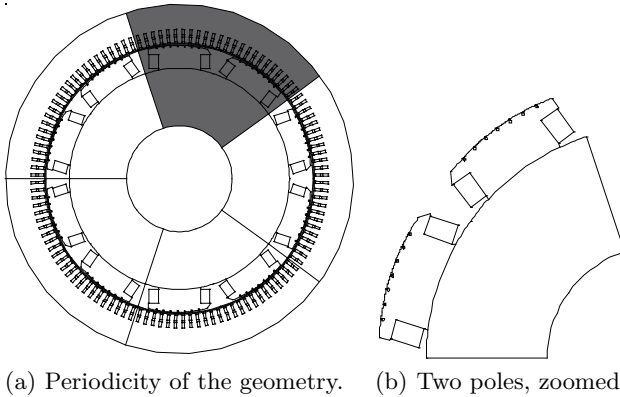

(a) Periodicity of the geometry.   (b) Two poles, zoomed.

Fig. 2.5. Cross-section.

The simulated fraction depends on the periodicity of the geometry of the rotor and on the periodicity of the stator winding. i.e. for a machine with an integer number of slot per pole and phase the fraction to simulate will be 1 pole pitch, if two consecutive pole shoes

are rotationally identical, or 2 pole pitches if they are alternatively shifted (fig. 2.5(b)). For a machine with a fractional number of slot per pole and per phase the fraction will be one fundamental period of the stator windings.

2.2.5 Slide-band

Finally one of the problems when dealing with electrical machine is joining the rotor and the stator mesh while enabling the movements of the rotor.

Several solutions have been proposed. The most common is to modify the mesh in the air gap at the beginning of each time step. It will be used in this work.

For the sake of completeness, it should be noted that the reference [25] describes the use of an unmeshed air gap, in which the flux density variation is given by an analytical function. It will not be used in this work.

2.3 Conclusions, requirement for the FE software

As a conclusion, the features of the FE software to be developed are summarized below. The number of the chapter, and a description of the example on which they are checked is added between brackets.

- Ability to deal with non-linear materials. (ch. 4, Single-phase transformer)
- Ability to take eddy currents into account. (ch. 4.2, Single phase transformer with massive conductor)
- Modifiable mesh in the air gap. (ch. 6, Slide-band and periodic limit conditions)
- Simulation of a fraction only of the machine by taking the symmetries into account. (ch. 6, Slide-band and periodic limit conditions)
- Ability to be linked to a grid solver e.g., SIMSEN.

As no experimental data was available, these features will be tested by simulating the same device both with Flux2D [26] and the developed program.

Flux2D was chosen as it is a reference in the world of the simulation of electrical machines with the FE. It is used by both machine manufacturer and utility companies to predict the behaviour of theirs machines. It should be noted, however, that the circuit simulations capability of Flux2D, while sufficient to carry out simulation pertaining to the machine itself (short-circuit, induced voltage waveform, etc.) are by no means able to take into account the complexity of a whole grid or a power converter along with its command and control. Also, at the beginning of this work, the ability to directly interface Flux2D and SIMSEN was lacking.

2.3.1 Software choice

The goal is to develop an FE program tailored to the task at hand. Nonetheless, existing software has been used for annex tasks. More specifically, the creation of geometries and their meshing make use of pre-existing software. Furthermore, the basic matrix arithmetic will be dealt with a commercial software library.

The geometry creation process is illustrated by (fig. 2.6). The first geometries studied (single phase transformer, without (fig. 4.1), and with bar (fig. 4.8)) were very simple. They were created by editing manually the files describing their nodes, segments and regions. The elements were then created by an external mesher.

This method is clearly not usable with even slightly more complex geometry such as the simple synchronous machine dealt with in (ch. 6), cf. (fig. 6.1). It would however be easy to create these geometries using Flux2D, and then somehow writing the necessary files.

The automatization features of Flux2D were used to write these files. Flux enables the user to write small programs, called scripts, which can use all the function of the geometry creation. These programs are written in Python and executed directly in Flux2D by an
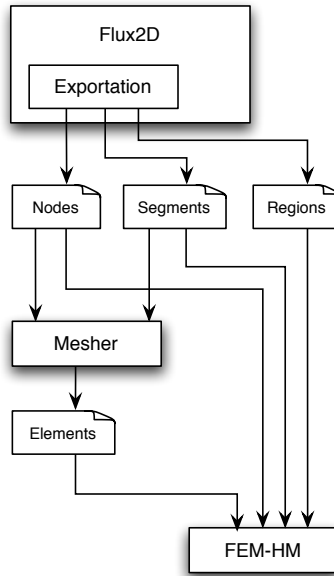
Fig. 2.6. Creation of the geometries.

embedded interpreter. The interesting point is that all the functions of Python are available including the file input / output routine.

Now the geometries are created with Flux2D then the necessary files are written by an exportation routine. The external mesher have been retained as the exportation of the mesh created by Flux2D is, perhaps oddly, much more difficult than the exportation of the geometry.

The mesher used is called 'Triangle'. It was developed at University of California Berkeley and is available under the GNU software license.

The last task involving pre-existing software is the matrix arithmetic. Countless libraries have been written to tackle this problem and it would be a real waste of time to write one's own. Here this problem is dealt with using MtxVec [27], a software package that encapsulates the standard LAPACK [28] library used for basic linear algebra operations and the UMFPACK [29] solver for large, sparse, linear systems. Both of these libraries have been chosen because they are widely used in industrial applications.

3

Field equations

This chapter introduce the FE equations and how they will be solved. A first section deals with the discretization of Maxwell's equations. Then the linking methods are described and finally the time resolution method used is presented.

3.1 Field equations

This chapter describes the equation solved by the finite elements method. This topic has been covered by an extensive litterature (e.g. [24, 30, 31]), so only a basic introduction is provided here.

From the electrical point of view, there has three different kinds of regions: The insulating regions (air, insulation, laminated iron) in which no current flows, the windings in which the currents is homogeneous and finally the damper bars which exhibit eddy currents. Each of these regions will call for a slightly different equations set, which will be set up in the next paragraphs. As the windings and bars are part of an external circuit, expressions linking the circuit and FE domain are also provided. They are the induced voltages in the case of the windings and the induced currents in the case of the solid conductors.

A remark on the notation first. The vector variables are written in bold.

Starting with Maxwell's equations (3.1- 3.4), first the displacement current is neglected in front of the conduced current, as the frequency is low enough. Then the flux density **B** is replaced by the vector potential **A**, defined by $\nabla \times \mathbf{A} = \mathbf{B}$. This substitution is usual when dealing with two dimensional problems as it allows to reduce the amount of unknowns.

$$\nabla \times \mathbf{E} = -\frac{\partial \mathbf{B}}{\partial t} \tag{3.1}$$

$$\nabla \times \frac{\mathbf{B}}{\mu} = \frac{\partial(\varepsilon \mathbf{E})}{\partial t} + \mathbf{J} \tag{3.2}$$

$$\nabla \cdot (\varepsilon \mathbf{E}) = \rho_q \tag{3.3}$$

$$\nabla \cdot \mathbf{B} = 0 \tag{3.4}$$

Therefore the equations (3.1) and (3.2) can be rewriten as (3.5) and (3.6)

$$\nabla \times \mathbf{E} = -\frac{\partial}{\partial t} \nabla \times \mathbf{A} \tag{3.5}$$

$$\nabla \times \frac{\nabla \times \mathbf{A}}{\mu} = \mathbf{J} \tag{3.6}$$

The first equation can be further transformed to get (3.7).

$$\nabla \times \left(\mathbf{E} + \frac{\partial}{\partial t} \mathbf{A} \right) = 0 \tag{3.7}$$

Therefore it is possible to introduce the electrical potential, defined by (3.8)

$$-\nabla V = \mathbf{E} + \frac{\partial \mathbf{A}}{\partial t} \tag{3.8}$$

Hence the electrical field is given by equation (3.9).

$$\mathbf{E} = -\frac{\partial \mathbf{A}}{\partial t} - \nabla V \tag{3.9}$$

3.2 2D hypothesis

In a 2D magnetic problem, the current flows along one axis and the flux density lays in the plane perpendicular to it. The unknown **B** has thus two components. The choice of the vector potential enables reducing the unknown to a scalar.

If the permeability is piecewise uniform, then (3.6) can be rewritten as (3.10). This latter expression is further reduced to (3.11), upon the gauge choice $\nabla \cdot \mathbf{A} = 0$. (Gauge choices are discussed in [32] and [33])

$$\frac{1}{\mu}\left(\nabla(\nabla \cdot \mathbf{A}) - \nabla^2 \mathbf{A}\right) = \mathbf{J} \qquad (3.10)$$

$$-\frac{1}{\mu}\nabla^2 \mathbf{A} = \mathbf{J} \qquad (3.11)$$

As the currents flow strictly along the z axis (3.11) becomes simply (3.12), where A and j are respectively the component of the vector potential and the current density along the z axis.

$$-\frac{1}{\mu}\nabla^2 A = j \qquad (3.12)$$

It follows from the previous development that the unknown is the component of the vector potential along the z axis, designated A. Accordingly, A_k is the value of the z component of the vector potential on the k- th node of the mesh.

3.3 Approximation of the vector potential

The approximation of the vector potential coming from an FE computation is based on the so called "form functions". These functions are defined as follow:

There is one form function for each node in the mesh. The function $\alpha_i(x, y)$ which depends on the node i of the mesh has the value 1

at that node and 0 at every other. For this work it has been decided to use linear form function i.e., their value varies linearly between the node to which they belong and the neighbouring nodes. An example of these functions, on an hypothetical 6 nodes mesh, is shown on (fig. 3.1).
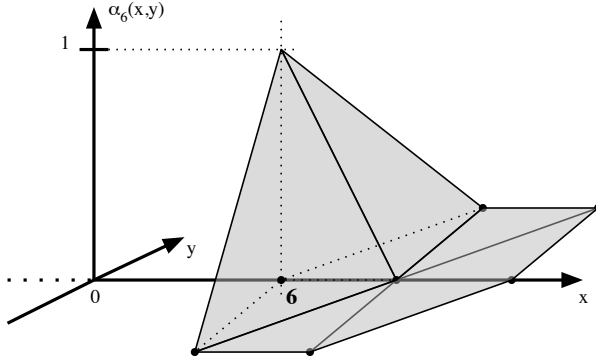

Fig. 3.1. Form function of node 6.

Then, the approximation of the vector potential has the form of (3.13), where A_i are the values of the vector potential at each of the node of the mesh. It follows from (3.13), that within an element, the vector potential is approximated by a piece of a plane (fig. 3.2).

$$A(x,y) \sum_{i=1}^{n} A_i \cdot \alpha_i(x,y) \tag{3.13}$$

It can then be inferred from $\mathbf{B} = \nabla \times \mathbf{A}$, that the flux density is uniform on an element, and so is the permeability. This verify the hypothesis made at the previous section on the local uniformity of the permeability.
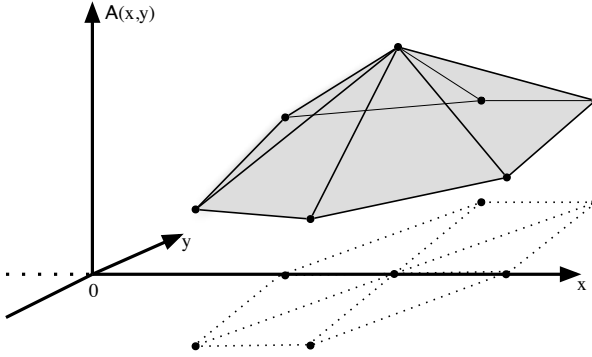
Fig. 3.2. Approximation of the vector potential.

3.4 Non- conducting regions

By definition, no current flows through these regions, henceforth the current is set to 0 in equation (3.6).

$$-\frac{1}{\mu}\nabla^2 A = 0 \tag{3.14}$$

3.5 Windings

It is assumed that the wire they are made of is too thin to be affected by eddy currents. Consequently, the current density carried by a region of surface s, with m turns, through which flows a current i is simply $j = \frac{m \cdot i}{s}$ and (3.6) becomes (3.15)

$$-\frac{1}{\mu}\nabla^2 A = \frac{m \cdot i}{s} \tag{3.15}$$

The equation (3.15) is then discretized with the FE method to get (3.16). If one assumes a mesh with n nodes where the vector potential

is free to vary and a device with p windings, then M is an $n \times n$ matrix whose entries depend on the shape of the elements and on the value of the permeability and N is an $n \times p$ matrix whose entries depend on the shape of the elements and on the number of turns of the windings. The unknowns $A_1 \cdots A_n$ are the nodal values of the vector potential i.e., the z component of the potential vector at each of the mesh's nodes. It should be noted that if saturable material are taken into account (i.e. $\mu(H)$) then the system of equations (3.16) is non-linear.

$$M(\mu) \cdot \begin{bmatrix} A_1 \\ \vdots \\ A_n \end{bmatrix} = N \cdot \begin{bmatrix} i_1 \\ \vdots \\ i_p \end{bmatrix} \tag{3.16}$$

The total voltage at the terminals of a winding is given by the usual formula $u_s = R \cdot i + \frac{d\psi}{dt}$. The equivalent circuit of a winding is thus shown on (fig. 3.3).
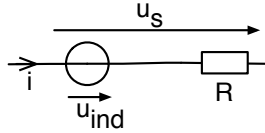

Fig. 3.3. Equivalent circuit of a winding ($u_i = d\psi/dt$).

The total flux ψ is computed from the vector potential. If one assumes a single turn coil, the flux through it is given by equation (3.17)

$$\iint_{\Sigma} \nabla \times \mathbf{A} \cdot d\mathbf{s} = \oint_{\partial \Sigma} \mathbf{A} \cdot d(l) = \Phi \tag{3.17}$$

In the 2D approximation used the vector potential is integrated on the path Σ defined on (fig. 3.4). As the potential is perpendicular

to the path on the segment l_2 and l_4, the flux becomes,

$$h(A_1 - A_3) = \Phi \qquad (3.18)$$

where h is the equivalent length of the model. The flux on a coil with several turns is computed in the same way. The figure (3.5) shows a m-turn coil whose strands are spread across the surface s_1 and s_2. On the surface s_1 the current is positive if it flows in the direction of z. On s_2 it is positive if it flows in the opposite direction. In this case, however, the position of each wire is unknown. As a consequence, it is assumed that each wire sees the mean vector potential on the surface s_1 and s_2, $\tilde{A}_1$ and $\tilde{A}_3$ respectively. And thus the voltage induced in the coils is given by,

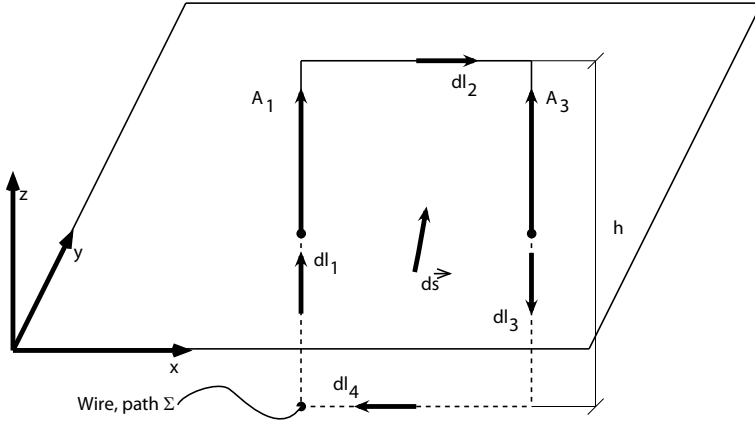$$u_i = mh\frac{d}{dt}\left(\tilde{A}_1 - \tilde{A}_3\right) \qquad (3.19)$$
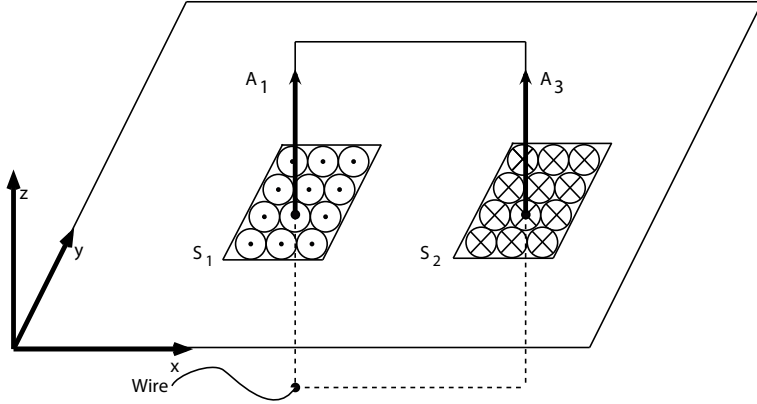

Fig. 3.4. Single turn coil.

Fig. 3.5. Multi-turn coil.

The induced voltage in a winding is obtained from the nodal potential vector by (3.20), in which the matrix T depends on the shape of the elements, the number of turn of the windings and on the equivalent depth of the problem.

$$T \cdot \frac{d}{dt} \begin{bmatrix} A_1 \\ \vdots \\ A_n \end{bmatrix} = \begin{bmatrix} u_{ind,1} \\ \vdots \\ u_{ind,p} \end{bmatrix} \tag{3.20}$$

It should be noted that the multiplication by T actually accomplishes two tasks. It first computes the average of the vector potential on the regions which make up the coil and multiply it with mh. This yields the flux on each region. It then sums the contributions of the regions to give the total flux seen by the coil. The same principle applies if the winding is made of more than two regions.

3.6 Eddy currents regions

Their section is large enough to carry eddy current, thus the current density is unknown. By replacing j by the the electrical field (3.9) in (3.6), this latter equation becomes (3.21). Notice that in this case, the source term is a function of the total voltage across the bar.

$$-\frac{1}{\mu}\nabla^2 A + \sigma\frac{\partial \mathbf{A}}{\partial t} = \sigma\frac{u_s}{h} \qquad (3.21)$$

The discretized form of (3.21) is (3.22). It really is the same expression than (3.16) with an added term K. On the same hypothetical mesh than before, K is a $n \times n$ matrix whose entries depend on the shape of the elements as well as the conductivity. If, this time, q solid conductors are considered instead of the windings, the matrix S is an $n \times q$ matrix whose entries depend on the conductivity of the bars and on the equivalent length of the problem.

$$K \cdot \frac{d}{dt}\begin{bmatrix} A_1 \\ \vdots \\ A_n \end{bmatrix} + M(\mu) \cdot \begin{bmatrix} A_1 \\ \vdots \\ A_n \end{bmatrix} = S \cdot \begin{bmatrix} u_1 \\ \vdots \\ u_q \end{bmatrix} \qquad (3.22)$$

The equivalent circuit of an eddy current region is shown on (fig. 3.6). For this kind of regions it is assumed that the voltage applied to their extremities (u_s) is given by the circuit equations. Hence, an expression for total the current flowing through them is needed. For a given bar, this expression (3.23) is obtained by integrating the electric field (3.9) on the surface s of the bars

$$j_{tot} = -\sigma\frac{\partial \mathbf{A}}{\partial t} - \sigma\nabla V$$

$$i_{tot} = -\sigma\iint_s \frac{\partial \mathbf{A}}{\partial t}\,ds + \frac{u_s}{R} \qquad (3.23)$$

where $R = \frac{h}{\sigma s}$ is the bar's resistance and u_s the total voltage applied at its extremities. On the right-hand side the first term is the
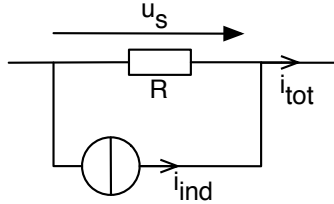
Fig. 3.6. Equivalent circuit of an eddy current region.

induced current, whereas the second is the source term. The induced current is computed from the nodal potential vector by (3.24). The entries of the matrix C depends on the shape of the elements and the conductivity of the bars.

$$\begin{bmatrix} i_{ind,1} \\ \vdots \\ i_{ind,q} \end{bmatrix} = C \cdot \frac{d}{dt} \begin{bmatrix} A_1 \\ \vdots \\ A_n \end{bmatrix} \quad (3.24)$$

3.7 Linking method

This section presents the methods used to add an FE model to SIMSEN, the so-called "linking methods".

The name itself implies that there are two independent entities SIMSEN and an FE software with something in between, the link whose nature will be discussed here. However, the first idea that comes to mind is to treat the FE model no differently than the modules already implemented and not use a link at all.

This idea is explored in the first section below. It also gives a rational as to why a linking method is needed. Then, two linking methods are described. Application examples follow in the next chapters.

3.7.1 Direct link

With this method, the FE models are treated like every other modules of SIMSEN. The FE equations are concatenated with the circuit equations in a single system (fig. 3.7), which is then solved by SIMSEN.
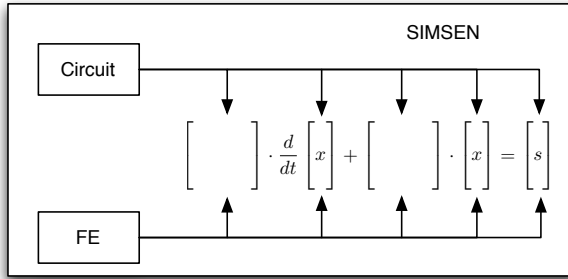

Fig. 3.7. Including an FE model in SIMSEN itself.

Compared to the other methods it has two advantages: it only requires a single FE resolution at each time step and does not add error to the solving process.

However, it has two deficiencies that renders it unusable in practice. First, the solver of SIMSEN uses a direct method to solve linear equations systems. This procedure has been tested with, at the most, 2000 variables, whereas an FE modelling of an electrical machine routinely has 10 000 to 20 000 variables. So this direct procedure, which is of adequate speed for a strictly electrical problem, will likely be too slow with a problem up to ten time as big.

The second problem is related to the algorithm used to solve the time dependant equations system. SIMSEN offers a choice of three different methods, namely: forward Euler, Runge-Kutta 3 and

Runge-Kutta 4. To solve a differential equation of the form $D \cdot \dot{\mathbf{x}} + G \cdot \mathbf{x} = \mathbf{s}$, all of these three methods need D to be regular. More specifically they all need an expression of the form $\mathbf{x^{k+1}} = D^{-1}(...)$.

Now, it is clearly seen from (3.22) that the matrix K is not regular i.e., for all the nodes which are outside of solid conductors, the corresponding line in the matrix K is identically null. Therefore any combination of circuit and FE equations will lead to a matrix D which is irregular and the three solvers offered by SIMSEN are unsuited for this kind of problem.

Then, directly adding the FE model in SIMSEN as if it were simply another module is clearly not an option, as it would require both to change the type of time solver and to change the linear solver used in SIMSEN.

This procedure has nevertheless been kept for debugging purpose. In this case the circuit (usually simple sine sources) and the FE equations are solved together with the backward Euler method.

3.7.2 Differential inductances

This linking procedure is based on the following idea: In the circuit solver, each winding is modelled as an inductor coupled with all the other windings.

The simulation progresses in interlocking steps. First, a set of inductances is computed with the finite element. Then, using these inductances, a time step is computed by the circuit solver, which yields a new configuration of currents, and the whole process is repeated until the final time is reached. The figure (3.8) illustrates this method.

In a device comprising n winding, the voltage at the terminals of the winding k is given by equation (3.25). where R_k, i_k, Ψ_k are respectively the resistance, current, and total flux seen by the winding k.

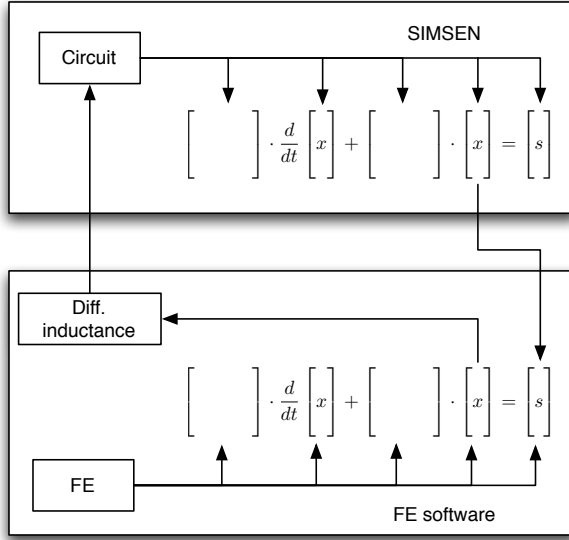$$u_k = R_k i_k + d\Psi_k/dt \qquad (3.25)$$

Fig. 3.8. Link with differential inductances.

As the currents are used as state variables, the flux derivative is expanded as (3.26).

$$u_k = R_k i_k + \sum_{j=1}^{n} \frac{\partial \Psi_k}{\partial i_j} \frac{di_j}{dt} \tag{3.26}$$

The factor $\partial \psi_k / \partial i_j = L_{k,j}$ is the differential inductance of the winding k with respect to the current j, (3.25) can therefore be rewritten as (3.27).

$$u_k = R_k i_k + \sum_{j=1}^{n} L_{k,j} \frac{di_j}{dt} \tag{3.27}$$

For this first test the differential inductances were computed by a first order centred numerical approximation(3.28). Therefore two resolution FE are needed for each winding.

$$L_{k,j} = \frac{\Psi(i_1, ..., i_j + \Delta i_j, ..., i_n) - \Psi(i_1, ..., i_j - \Delta i_j, ..., i_n)}{2\Delta i_j} \quad (3.28)$$

It should however be noted that the reference [34] presents a method for the computation of the differential inductance based on an analytical sensibility method, which only requires a single resolution for the computation of all the differential inductances of a given FE model.

Rotating windings

The previous equation (3.27) is valid if the variation of the flux is solely the result of a variation of the currents. However, in the presence of a rotating winding (e.g., the field winding of a synchronous machine), the rotation itself causes a change in the flux. Thus (3.27) has to be amended to take into account the derivative of the flux with respect of the position of the rotor (3.29).

$$u_k = R_k i_k + \sum_{j=1}^{n} L_{k,j} \frac{di_j}{dt} + \frac{d\Psi_k}{d\alpha} \cdot \dot{\alpha} \quad (3.29)$$

This last derivative can be computed by a forward approximation (3.30). This means that at each time step an additional FE computation is performed with the same current configuration but with the rotor rotated of an additional angle $\Delta\alpha$.

$$\frac{d\Psi_k}{d\alpha} \approx \frac{\Psi_k(\alpha + \Delta\alpha) - \Psi_k(\alpha)}{\Delta\alpha} \quad (3.30)$$

3.7.3 Newton-Raphson

This linking method is based on the following idea. If both of the voltage sources on (fig. 3.9) have the same value and this value is adapted so that the currents i_c and i_{fem} are equal, then the situation is formally the same as the one described on (fig. 3.10).
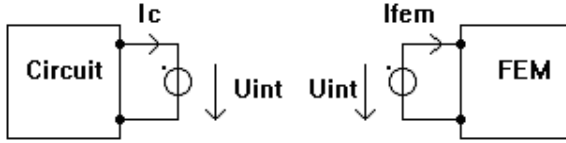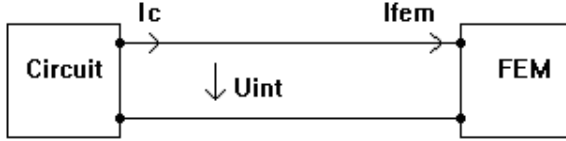

Fig. 3.9. Coupling principle.

Fig. 3.10. Equivalent coupled system.

So at each time-step the goal is to find u_{int} such as $i_c(u_{int}) = i_{fem}(u_{int})$. This latter equation can be rewritten as (3.31). And the value of u_{int} that satisfy $\varepsilon = 0$ is obtained by the Newton-Raphson method. i.e. a series of values for u_{int} is build so that the $n + 1$- th value is given by (3.32), where ε' is the derivative of ε with respect to u_int. The principle of this linking method is shown on (fig. 3.11).

$$\varepsilon(u_{int}) = i_c(u_{int}) - i_{fem}(u_{int}) \qquad (3.31)$$

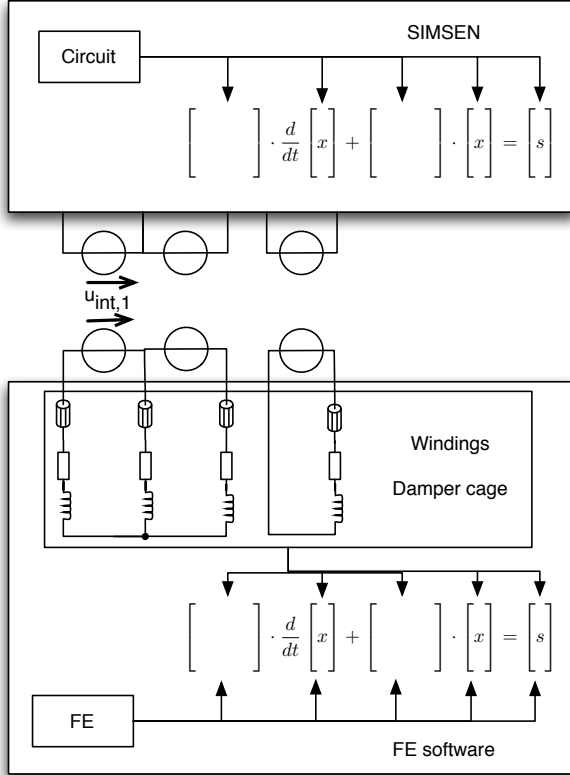$$u_{int,n+1} = u_{int,n} - \frac{\varepsilon(u_{int,n})}{\varepsilon'(u_{int,n})} \qquad (3.32)$$

Fig. 3.11. Link with the Newton-Raphson method.

If more than one current is linked, (3.32) becomes (3.33), where D is the Jacobian matrix of the function $\boldsymbol{\varepsilon_n}(\mathbf{u_{int}})$ The major drawback of this method is readily apparent i.e., the Jacobian matrix (3.34) have to be updated at each iteration. This update requires $2k^2$ FE computations, where k is the number of linked currents.

$$\mathbf{u_{int,n+1}} = \mathbf{u_{int,n}} - \mathbf{D}^{-1}\varepsilon(u_{int,n}) \qquad (3.33)$$

$$\mathbf{D}\left(\boldsymbol{\varepsilon}_n\right) = \begin{bmatrix} \frac{\partial\varepsilon_1}{\partial u_{int,1}} & \cdots & \frac{\partial\varepsilon_1}{\partial u_{int,k}} \\ \vdots & \ddots & \vdots \\ \frac{\partial\varepsilon_k}{\partial u_{int,1}} & \cdots & \frac{\partial\varepsilon_k}{\partial u_{int,k}} \end{bmatrix} \qquad (3.34)$$

To reduce the number of FE computation needed at each time-step, it is possible to use the Newton-secant method, a variant of the Newton-Raphson method. With the former method the Jacobian matrix is computed only at the beginning of each time step, not during the iterations of the Newton-Raphson method itself. This dramatically reduces the number of FE computation needed at the price of a slower convergence.

Finally, the algorithm for solving a time-step with the Newton-secant method is shown on (fig. 3.12). Starting with the currents and intermediate voltages obtained at the previous step, the Jacobian matrix is computed. Then new values for the currents, error and intermediate voltages are computed. These last three operations are repeated until the error is smaller than a given tolerance.

3.8 Time resolution

The differential inductances and Newton-Raphson linking methods both need a time resolution in the FE program. The time solver used is discussed here.

The complete equations set (3.35) modelling the machine is made of the FE equations and the circuit equations of the windings and
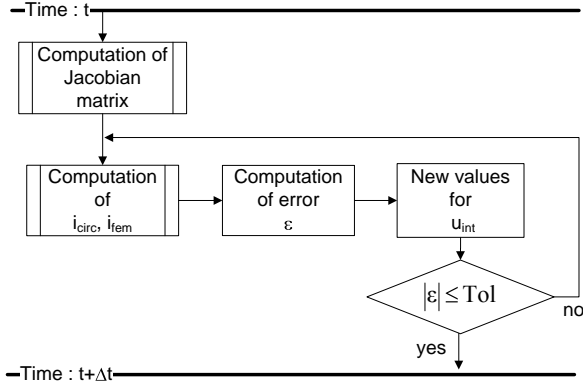
Fig. 3.12. Newton-secant algorithm.

damper cage. The unknowns $x_1 \cdots x_k$ are the nodal values of the potential vector and the circuit variables.

The exact content of the matrices $\mathbf{Q}$ and $\mathbf{G}$ depends on the modelled device. However, it is readily apparent from (3.16) and (3.22) that the complete equations set is heterogeneous i.e., it is made of both differential and algebraic equations.

This property influences the choice of the solver for the time resolution. As the matrix $\mathbf{Q}$ is irregular all solvers that require an expression for $\frac{d}{dt}[x_1 \cdots x_k]'$ are not usable. For this reason, along with its unconditional stability and ease of implementation the backward Euler method has been chosen.

$$
\mathbf{Q} \cdot \frac{d}{dt}
\begin{bmatrix} x_1 \\ \vdots \\ x_k \end{bmatrix}
+ \mathbf{G} \cdot
\begin{bmatrix} x_1 \\ \vdots \\ x_k \end{bmatrix}
=
\begin{bmatrix} v_1 \\ \vdots \\ v_k \end{bmatrix}
\tag{3.35}
$$

3.8.1 Non-linear solver

As (3.35) is solved by the backward Euler method at each time step, the equations system (3.36) is solved.

$$(\mathbf{Q} + \mathbf{G} \cdot \Delta t) \begin{bmatrix} x_1^{n+1} \\ \vdots \\ x_k^{n+1} \end{bmatrix} = \mathbf{Q} \cdot \begin{bmatrix} x_1^n \\ \vdots \\ x_k^n \end{bmatrix} + \begin{bmatrix} v_1^{n+1} \\ \vdots \\ v_k^{n+1} \end{bmatrix} \Delta t \qquad (3.36)$$

This equations system is non-linear since the matrix $\mathbf{G}$ contains $M(\mu)$. It is solved by an iterative algorithm.

At each iteration a new value for the unknowns and for the permeability is computed. On any of the element let us consider that the previous iteration i was computed with the value μ_i of the permeability and yields the flux density B_i (fig. 3.13). Now, the point $(H_i = B_i/\mu_i;\ B_i)$ may not lay on the magnetic curve $B(H)$. Then, the value of the permeability is updated by $\mu_{i+1} = \frac{B_i'(H_i)}{H_i}$. The same calculation are repeated on every elements that have a non-linear magnetic characteristic. After that, the entries of the matrix M are updated according to the new values of the permeability. This in turn leads to a new value for the matrix G. The equations system (3.36) is solved once again with this new matrix. The whole process is iterated until the stopping criterion (3.37) is satisfied on all the elements on which a non-linear magnetic characteristic is defined.

$$\frac{\mu_{i+1} - \mu_i}{\mu_{i+1}} < rTol \qquad (3.37)$$

The figure (3.14) shows the magnetic characteristics that have been used in this work. The models and the reference of the chapters they are used in, is given in (tab. 3.1).
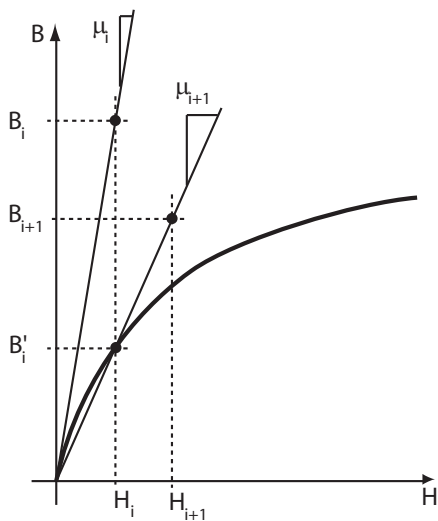
Fig. 3.13. Iteration on μ.

Curve name	Model	Chapter
Transformers	Single-phase transformer	4
	Single-phase transformer with bars	4
	Three-phases transformer	5
Induction machine	Induction machine	7
Hydro generator, rotor	Hydro generator	8
Hydro generator, stator	Hydro generator	8

Table 3.1.
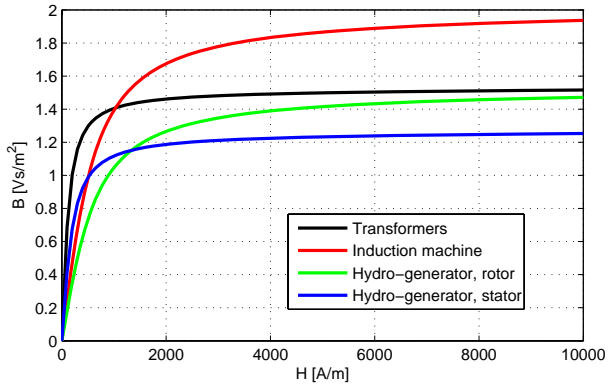
Fig. 3.14. Magnetic characteristics.

4

Single phase transformer

Before this work began, an FE program solving magneto-static problems with only linear material had already been written. Based on this results the next steps are to deal with non linear material and add to this program the ability to solve time dependant problems. Furthermore, a first test of the coupling method between the FE modeling and the external circuit is done. Finally two solid conductors are added to the transformer. This will allow to check the implementation of the discretized equation of the solid conductor (3.22). This chapter first deals with the simplest case (without bars), then from section 4.2 on, with bars.

The results were validated by comparing the currents with the ones computed with Flux2D.

4.1 Stranded windings

The test case used in this section is the turn-on of a loaded single phase transformer. The simulations were performed with three different modellings.

The first one uses differential inductance to link the circuit and FE solver. This is a logical choice as a first test as in the case of the

single phase transformer the differential inductances are obtained through magneto-static computation only.

In the second one the equations from the FE model and the feed circuit are solved together. This is a first check of the resolution of a time varying problem.

The third modelling makes a direct use of the previous case in that the circuit equations relative to the windings (e.g. induced voltage, resistive voltage drop and end winding inductance) were also added to the FE equations system. However, the feed and load circuits were simulated in a separate solver and the two solvers were linked by the Newton-Raphson method.

A note on the circuit solver: To avoid dealing with implementation issues yet, the solver used in these three simulations is not SIMSEN but a Runge-Kutta routine, that was compiled with the FE code itself.

4.1.1 Geometry

The transformer used in these test is a 373 [kVA] $18300[V]/242[V]$ single phase transformer . Its geometry is shown on (4.1). The chosen magnetic characteristic is shown on (fig. 3.14).

All the modelling share the same geometry, they only differ on the circuit used.

4.1.2 Differential inductances

The circuit used for this simulation (fig. 4.2) is straightforward. The resistors R_{add1} and R_{add2} are the total resistance of the primary and secondary winding respectively. The inductances L_{add1} and L_{add2} are the additional inductances needed to take into account the leakage not readily taken into account by the two dimensional FE model. A full discussion on the computation of these values is available in [23].
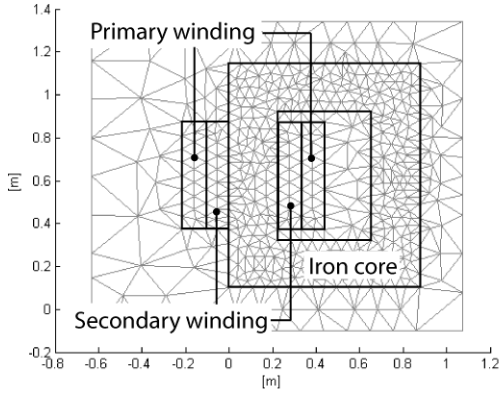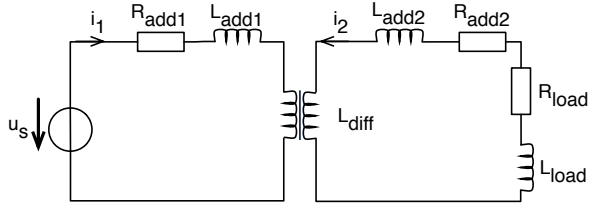
Fig. 4.1. Transformer.

Fig. 4.2. Coupling through differential inductances.

4.1.3 Direct link

In this case the FE and circuit equations are solved together in the same system. The equations set is derived from the equivalent circuit (fig. 4.3). Compared to the previous circuit the coupling between the two windings is now made by the two stranded components "winding1" and "winding2".
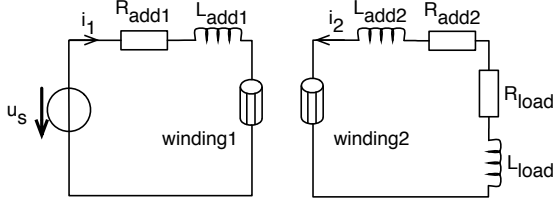
Fig. 4.3. FE and circuit equation solved together.

This time the necessary equations are: The discretized Ampere equation (3.16), then the definition of the induced voltage (3.20), and finally the circuit equations themselves (4.1).

$$M \cdot \begin{bmatrix} A \\ \vdots \\ A_n \end{bmatrix} = N \begin{bmatrix} i_1 \\ i_2 \end{bmatrix}, \qquad T \cdot \frac{d}{dt} \begin{bmatrix} A \\ \vdots \\ A_n \end{bmatrix} = \begin{bmatrix} u_{ind1} \\ u_{ind2} \end{bmatrix}$$

$$L_{add1} \frac{di_1}{dt} + u_{ind1} + R_{add1} i_1 = u_s$$

$$(L_{add2} + L_{load}) \frac{di_2}{dt} + u_{ind2} + (R_{add2} + R_{load}) i_2 = 0 \qquad (4.1)$$

4.1.4 Newton-Raphson

Both of the circuits used in this simulation are shown on (4.4). The upper part is solved by the circuit solver, whereas the lower part is solved along with the FE equations. The resistor R_{add1} is split between R_{circ1} and R_{fem1} such has $R_{circ1} + R_{fem1} = R_{add1}$. The inductance L_{add1} is similarly split. This is done to avoid having the two voltage sources u_s and u_{int1} in parallel.
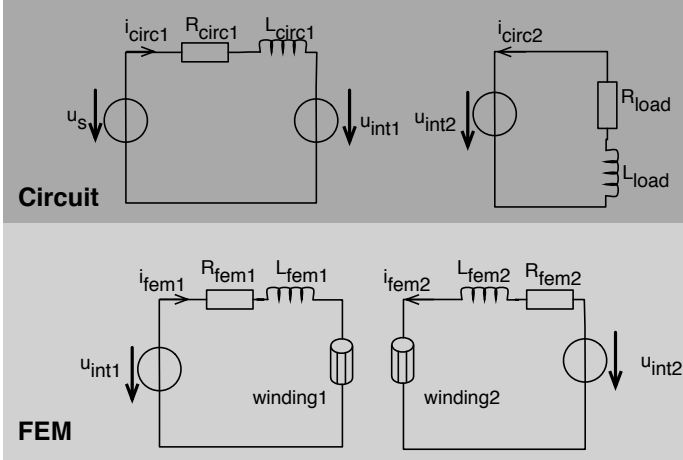
Fig. 4.4. Link by the Newton-Raphson method.

4.1.5 Simulations

Three test cases were simulated, the first one with a linear magnetic characteristic for the yoke steel, the other two with saturable steel: One in steady-state, the other one in transient.

A short transient after the switch-on is obtained by using the feed voltage $u_s = \sqrt{2} \cdot 18300 cos(\omega \cdot t)$, a longer transient by $u_s = \sqrt{2} \cdot 18300 sin(\omega \cdot t)$. This latter case also leads to high currents spikes and correspondingly to a wide variation of the magnetic saturation of the yoke, which makes it a good test case for the non-linear equations system solver. The influence of the phase of the feed voltage on the length of the transient is discussed in [35] p97, albeit for an unloaded transformer.

Linear magnetic characteristic

In this case the feed voltage $u_s = \sqrt{2} \cdot 18300 cos(\omega \cdot t)$ was chosen. The errors are summed up in (Tab. 4.1)

The currents are shown on (fig. 4.5). To keep the graph readable only the currents issued from Flux2D and the one linked by the Newton-Raphson method are shown.

Saturable steel yoke

As stated two simulations with a saturable yoke are presented. The first one is in steady-state. The currents (fig. 4.6) remain sinusoidal. The errors between Flux2D and the three different models are summed up in (Tab. 4.2).

Finally, the same simulation was carried out with a sine feed voltage. As predicted the currents (fig. 4.7) are heavily perturbed. The errors are summed up in (Tab. 4.3)
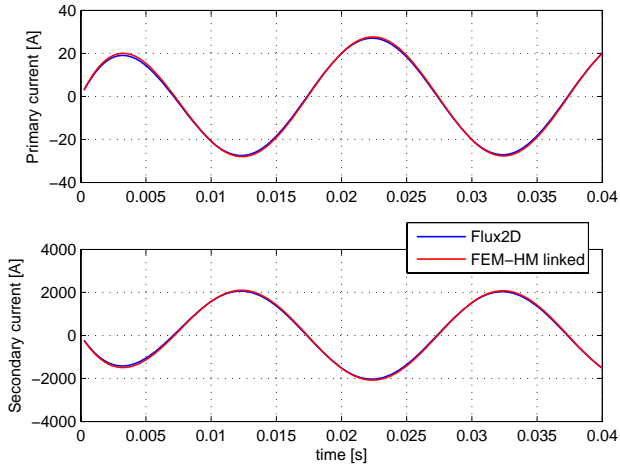
Fig. 4.5. Feed voltage cosine, linear yoke.

Reference		Primary current	Secondary current
Flux2D	Diff. inductances	0.49 %	0.48 %
	Direct	0.35 %	0.36 %
	Newton-Raphson	0.54 %	0.53 %
Direct	Newton-Raphson	0.36 %	0.36 %

Table 4.1. Cosine feed voltage, linear yoke.
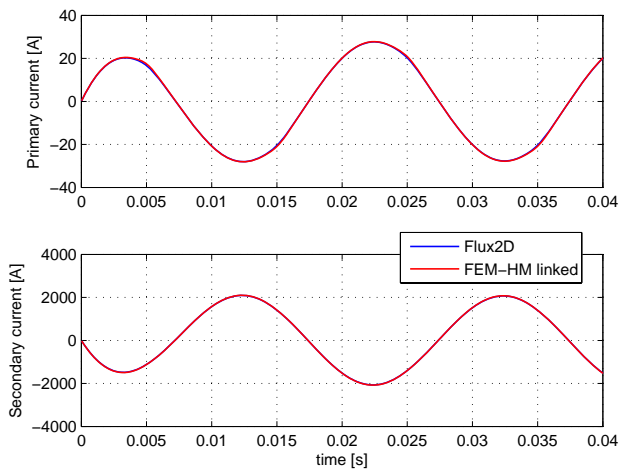
Fig. 4.6. Feed voltage cosine, saturable yoke.

Reference		Primary current	Secondary current
Flux2D	Diff. inductances	2.4 %	0.4 %
	Direct	2.0 %	0.2 %
	Newton-Raphson	2.9 %	0.5 %
Direct	Newton-Raphson	0.9 %	0.3 %

Table 4.2. Cosine feed voltage, saturable yoke.
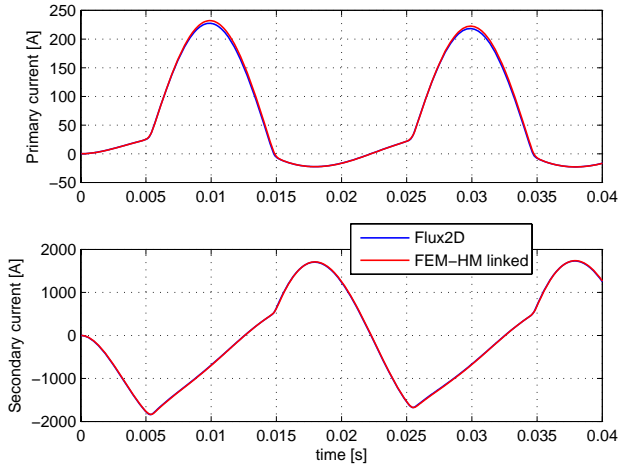
Fig. 4.7. Feed voltage sine, saturable yoke.

Reference		Primary current	Secondary current
Flux2D	Diff. inductances	2.4 %	0.62 %
	Direct	2.0 %	0.66 %
	Newton-Raphson	2.1 %	0.52 %
Direct	Newton-Raphson	0.42 %	0.39 %

Table 4.3. Sine feed voltage, saturable yoke.

4.2 Solid conductor

After the simulation of the single phased transformer the next step is to add solid conductors to the simulated system. This is by no means the modelling of an actual device. It will however allow to check the implementation of the discretized equation of the solid conductors (3.22).

4.2.1 Simulated system

The system studied in this chapter is essentially the single-phase transformer in chapter 4 to which two solid conductors were added.

It has been decided to let the bars be 3 time as wide as the skin depth for the material and the frequency used, so as to clearly show the different values of the current density within a bar. The skin depth [32] p62 is given by $\delta = \sqrt{2/(\omega\mu\sigma)}$. The bars are assumed to be made of copper with a conductivity of $\sigma_{Cu} = 59.5 \cdot 10^6 \, [1/(\Omega \cdot \text{m})]$, thus the skin depth is $\delta_{Cu} = 9.2 [mm]$.

The geometry used is shown on (fig. 4.8). The bars have been finely meshed (fig. 4.9) in order to accurately predict the eddy currents.

The accompanying circuit (fig. 4.10) is the same than the one used for the single-phase transformer with two added bars. The values of the components are the same than the one used for the single phase transformer. The circuit and FE equations have been solved together in the same system. No linking method has been used here, as the goal was to check the solver of the FE software itself.

4.2.2 Simulation and results

The same test cases than for the single-phase transformer are tried e.g: First the magnetic characteristic of the yoke is linear and the feed voltage is cosine. Then for the two next cases a saturable yoke is considered with a cosine then a sine feed voltage. The same consideration about the influence of the phase of the feed voltage on
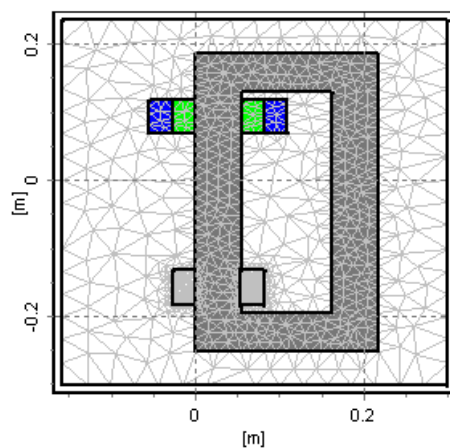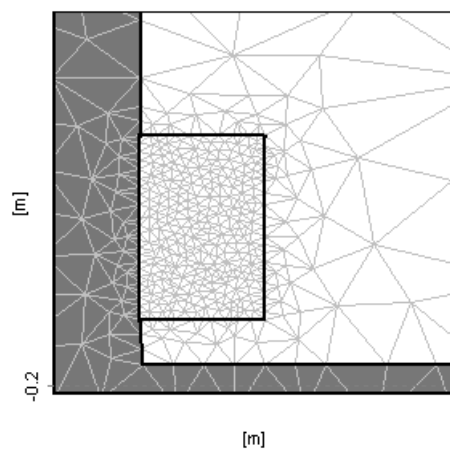
Fig. 4.8. Geometry.

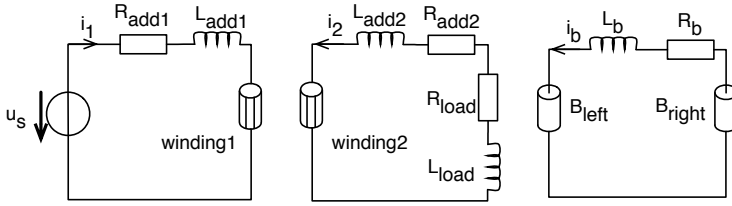**Fig. 4.9.** One bar, zoomed.

Fig. 4.10. Accompanying circuit.

the transient can be made. The cosine therefore yields the shortest transient, the sine a longer one.

Linear steel yoke

The goal of this simulation is to check the implementation of the matrices necessary for the simulation of solid conductors. Consequently, the steel of the yoke is linear to avoid eventual convergence problems and a cosine feed voltage is chosen in order to get a short transient.

The currents are shown on (fig. 4.11). The errors on the currents are 2.1 %, 1.3 % for the primary and secondary windings respectively and 2.5 % for the total current in the bars.

Saturable steel yoke

The first case simulated here is a switch-on with a cosine feed with null initial conditions.

Comparisons with Flux2D were made. The figure (4.12) shows the currents in the windings and the total current in the bars. The maximum errors between the program written and Flux2D are 4.1 %, 1.8 % for the primary and secondary windings respectively and 2.8 % for the total current in the bars.
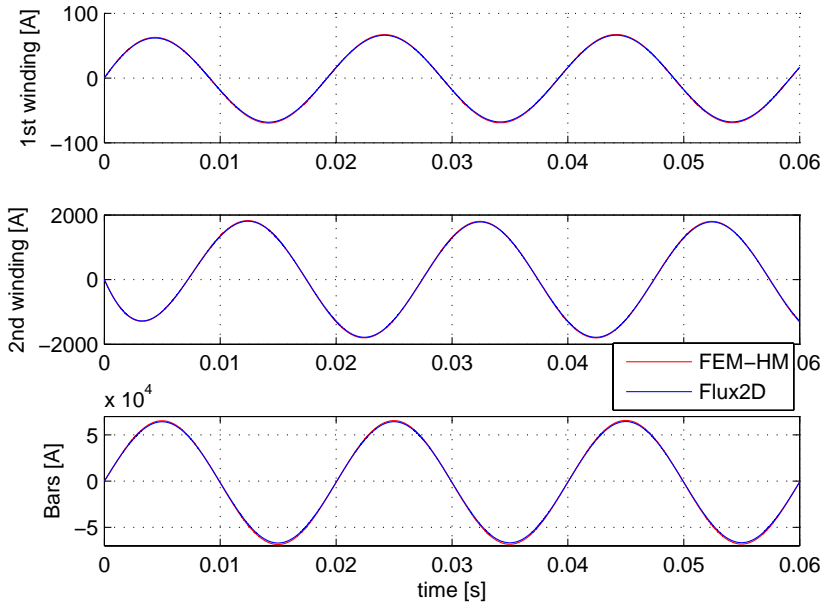
Fig. 4.11. Currents, linear yoke, cosine feed.

The main point of this simulation is, of course, the prediction of eddy currents. To this end the current density computed by FEM-HM and Flux2D were compared at four different instants spread over a fourth of a period. These comparisons are shown on (fig. 4.13) to (fig. 4.16). The color shade represents the data from FEM-HM, while the black contour lines are issued from Flux2D. The current density is said to be positive when it flows in the same direction than the z axis i.e., when it comes out of the page.

The second case is a sine switch-on. The currents are shown on (fig. 4.17). The maximal errors on the currents in the primary and secondary windings are 3.5 % and 2.9 % respectively. The errors on the currents in the bars is 2.5 %.
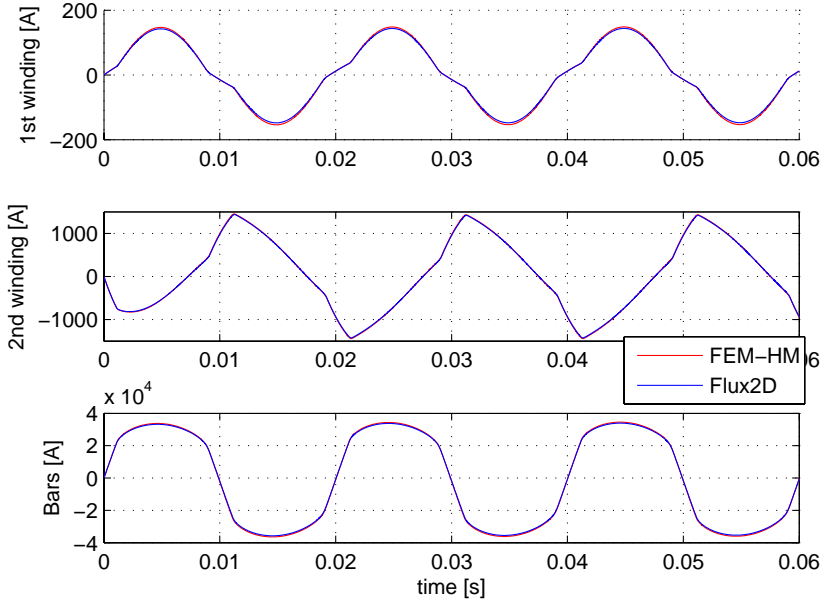
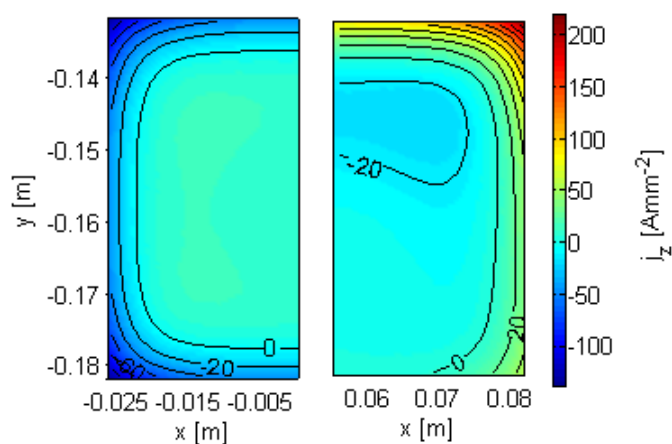

Fig. 4.12.   Currents, saturable yoke, cosine feed.

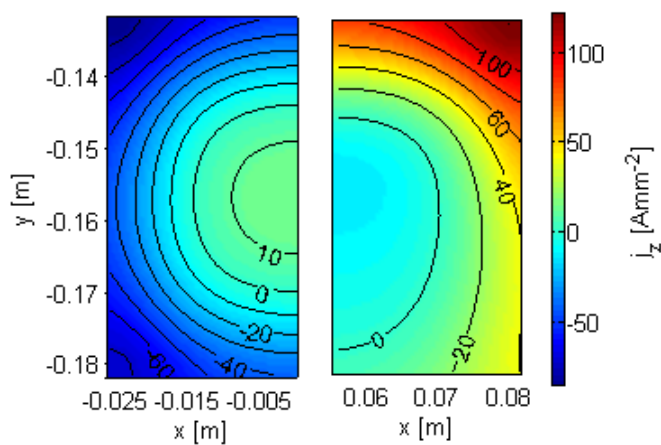**Fig. 4.13.** Current density at t=0.04 s.
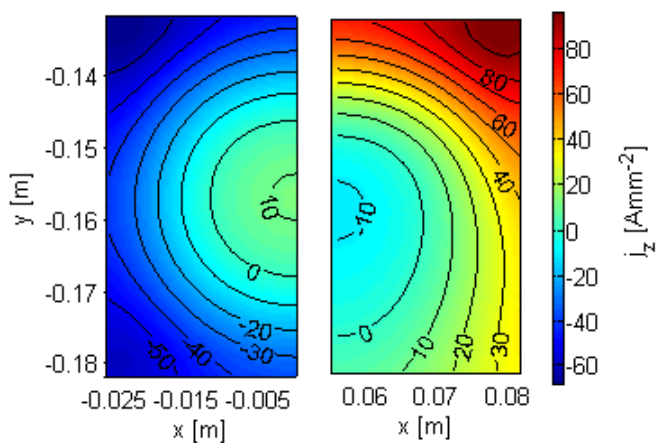

Fig. 4.14. Current density at t=0.043 s.

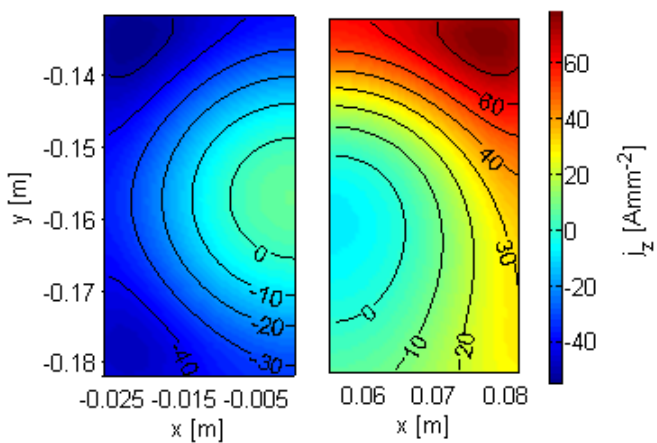**Fig. 4.15.** Current density at t=0.044 s.

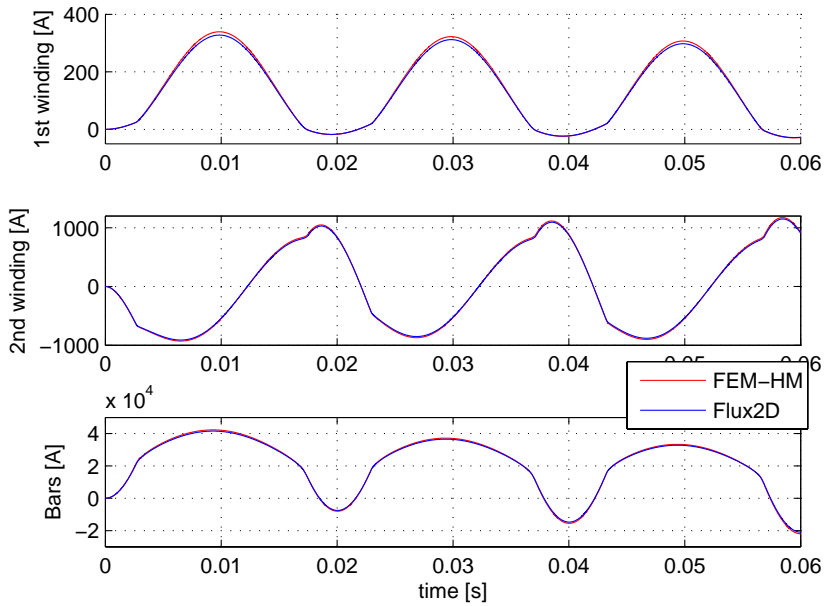**Fig. 4.16.** Current density at t=0.045 s.

Fig. 4.17. Currents, saturable yoke, sine feed.

4.3 Conclusion

4.3.1 Single-phase transformer

First the linear case with direct link (circuit and FE solved together) exhibits a maximal error of 0.36% compared to Flux2D. A perfect agreement could not be expected as the two simulations were made

using two different mesh, furthermore Flux2D uses second degree form function, whereas FEM-HM uses first degree ones.

Then, the error between the simulation without link, and the one in which two linked solvers are used is less than 0.4%. Once again, a perfect match was not expected as the algorithm allows for a 10^{-4} error between the currents on the circuit side, and those on the FE side. Hence the linking method is working.

Finally, in both of the saturated case the maximal error between the direct link and Flux2D is 2%. This added error compared to the linear case comes from the different algorithm used by Flux2D and FEM-HM to deal with the non-linearity. It should however be noted that this error has the same value in the case of a cosine and sine feed i.e., when the yoke is lightly, respectively strongly saturated. It can therefore be assumed that this error will remain reasonable for the next applications.

Choice of the linking method

As mentioned in (sect. 3.7.1) the "direct link" method cannot be used for actually embedding an FE model in SIMSEN. For debugging purpose, a simple circuit was in some cases added to the FE equations and the resulting system solved together. These cases are referred to as direct link in the next chapters.

Both the differential inductance and the Newton-Raphson method were used to solve the single-phase transformer. Both yielded good results. However this example made the shortcoming of the differential inductance method readily apparent.

The linking method has to be able to deal with any transient that can be simulated with equivalent circuit. A wide variation of the feed currents as it is the case with the sine voltage switch-on of the single-phase transformer leads to a correspondingly wide variation of the saturation of the yoke. This leads to wide and quick variations of the value of the differential inductances.

To take these variations accurately into account it has been found out that it is necessary to compute new values of the differential

inductances at each of the intermediate steps of the Runge-Kutta 4 method and use small time step, 10 $[\mu s]$ for the case of the sine switch-on. Failure to do so results in increasing discrepancy between the currents computed by Flux2D and FE-HM, and divergence.

The Newton-Raphson method can be used with a more reasonable time-step (0.1 [ms] was typically used for the simulations of this work) and communication is only necessary at the end of each time-step.

Furthermore, one troublesome problem with the differential inductance method is the computation of the derivative for both the inductance and the induced voltage coefficient in (3.29).

This arises with all numerical approximation of derivatives. The demeanor should be chosen small enough to accurately approximates the derivative, however doing so will yield two terms very close to each other for the numerator and the precision of the difference will suffer. This problem can be somewhat alleviated by computing the inductance without numerical approximation (cf. [34]), however the computation of the induced voltage term has to be carried out numerically.

Now, it may seem that the Newton-Raphson method suffers of the same trouble since a derivative is also needed for its computation. However, in this case the derivative is only used to compute the next step in an iterative procedure. Therefore any imprecision will affect the speed of convergence, not the quality of the results themselves.

4.3.2 Solid conductors

The simulation of a simple device with both solid and stranded conductor has been carried out. The error on the currents in both kind of conductors is in the same range than the error observed during the simulation of the transformer with only stranded windings. Furthermore, the current density in the solid conductors is accurately predicted. This shows that the additional terms introduced by the solid conductors (3.22) has been derived correctly from Maxwell's equations, and that their implementations are correct.

5

Three phases transformer

This chapter presents the simulation of a distribution transformer. Its rated values are: Power 1[MW], primary voltage 18'300[V], secondary voltage 242[V]. Both of its windings are star connected. It is a first step toward the simulation of rotating machine, as the stator of these machines and the primary of this transformer are both a three phases star connected windings.

The first goal is thus to check the implementation of the equations for a star connected circuit. The stability of the linking method is then tested with a discontinuous feed voltage. To this end, a square wave is fed to the transformer.

The solvers used are the same than for the single-phase transformer (sect. 4.1.4). Like this latter case, the circuit is split between a feed circuit and an accompanying circuit. The feed circuit is solved by the Runge-Kutta 4 method; the FE equations along with the accompanying circuit are solved with the backward Euler method. The solvers are linked by the Newton-Raphson method as described in (sect. 3.7.3).

5.1 Geometry and circuit

The geometry and mesh of the transformer are shown on (fig. 5.1). The primary windings are drawn in blue, the secondary windings, which are not used in these simulations, in green. Homogeneous Dirichlet boundary conditions are used on the outermost segments of the geometry.
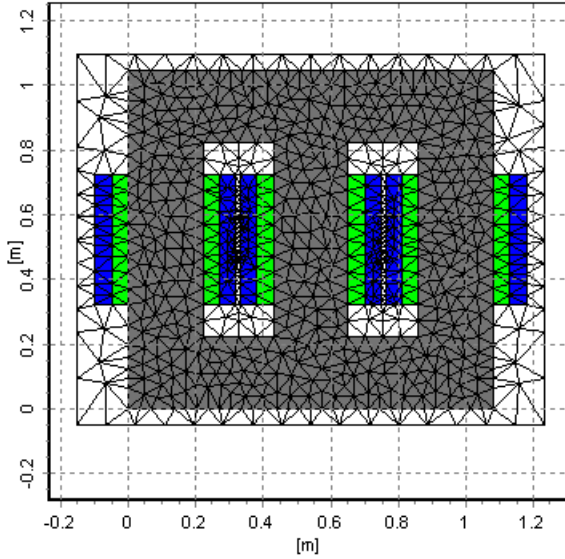

Fig. 5.1. Three-phase transformer, geometry.

The circuits used are shown on (fig. 5.2). The value of the windings resistance ($R_{add,1}$ for the first winding) is split between the feed circuit and the circuit accompanying the FE equations, such that $R_{add,1} = R_{fem,1} + R_{circ,1}$. The end winding inductance ($L_{add,1}$ for the first winding) is similarly split e.g., $L_{add,1} = L_{fem,1} + L_{circ,1}$.

As for the single-phase transformer, this was done to avoid having loops made only of voltage sources in the feed circuit.
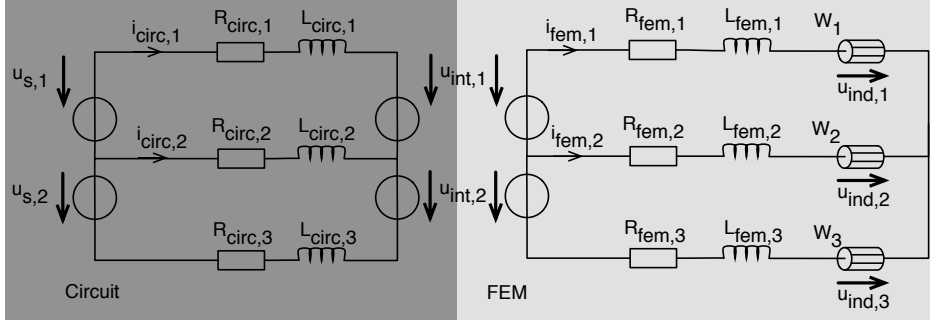

Fig. 5.2. Three-phases transformer, circuit.

Three groups of equations are solved by the FE solver. They are the electrical equations (5.1), the discretized Ampere's equation (5.2) and the link between the two the induced voltages (5.3).

$$
u_{int,1} = u_{ind,1} - u_{ind,2} + L_{fem,1} \cdot \frac{di_{fem,1}}{dt} - L_{fem,2} \cdot \frac{di_{fem,2}}{dt}
$$
$$
+ R_{fem,1} \cdot i_{fem,1} - R_{fem,2} \cdot i_2
$$
$$
u_{int,2} = u_{ind,2} - u_{ind,3} + (L_{fem,2} + L_{fem,3})\frac{di_{fem,2}}{dt} + L_{fem,3} \cdot \frac{di_{fem,1}}{dt}
$$
$$
+ (R_{fem,2} + R_{fem,3})i_{fem,2} + R_{fem,2} \cdot i_{fem,1} \qquad (5.1)
$$

$$
M \cdot \begin{bmatrix} A \\ \vdots \\ A_n \end{bmatrix} = N \begin{bmatrix} i_{fem,1} \\ i_{fem,2} \\ -i_{fem,1} - i_{fem,2} \end{bmatrix} \qquad (5.2)
$$

$$T \cdot \frac{d}{dt} \begin{bmatrix} A \\ \vdots \\ A_n \end{bmatrix} = \begin{bmatrix} u_{ind,1} \\ u_{ind,2} \\ u_{ind,3} \end{bmatrix} \tag{5.3}$$

On the feed circuit side, the equations solved are simply (5.4).

$$u_{s,1} - u_{int,1} = R_{circ,1}i_{circ,1} - R_{circ,2}i_{circ,2}$$
$$+ L_{circ,1}\frac{di_{circ,1}}{dt} - L_{circ,2}\frac{di_{circ,2}}{dt}$$
$$u_{s,1} - u_{int,2} = (R_{circ,2} + R_{circ,3})i_{circ,2} + R_{circ,3}i_{circ,1}$$
$$+ (L_{circ,2} + L_{circ,3})\frac{di_{circ,2}}{dt} + L_{circ,2}\frac{di_{circ,2}}{dt} \tag{5.4}$$

5.2 Simulations and Results

The two simulation carried out are switch-on from null initial conditions, with an open secondary.

Two feed voltages were tried. The first one is a cosine wave at nominal voltage, $u_{s,1} = \sqrt{2} \cdot 18300 \cdot cos(\omega t)$ [V]. The second one is a square shaped wave (fig. 5.4) similar to the one produced by a 6 transistors bridge with a 120 °switching sequence [36] on a purely resistive load.

The same simulations were carried out with Flux2D and their results compared with the ones obtained with FEM-HM.

The results are shown on (fig. 5.3)and (fig. 5.5) respectively. The tables (tab. 5.1) and (tab. 5.2) contain the maximal error between Flux2D and FEM-HM.
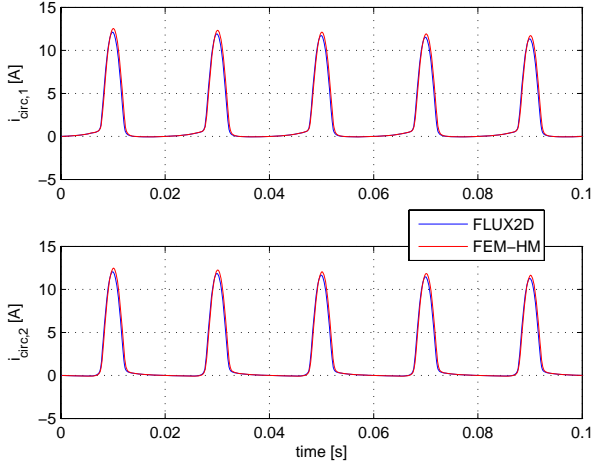
Fig. 5.3. Primary currents, switch on with cosine feed, open secondary.

Current i_1	Current i_2
5.7%	5.7%

Table 5.1. Error on the primary currents, switch on with cosine feed, open secondary.
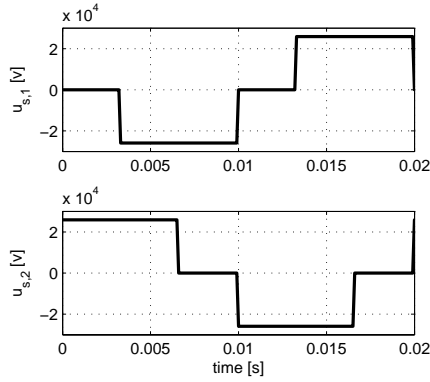
Fig. 5.4. Feed-voltage, square wave.

Current i_1	Current i_2
14.5%	7.5%

Table 5.2. Error on the primary currents, switch on with square wave feed, open secondary.

5.3 Conclusion

5.3.1 Cosine feed

The curves issued from FEM-HM closely follow the ones from Flux2D. Even if the agreement is not as good as the one obtained during the simulation of the single phase transformer (the maximum error being 5.7% three phases compared to 3% single phase), it is nevertheless possible to conclude that the implementation of the three phases circuit is correct.
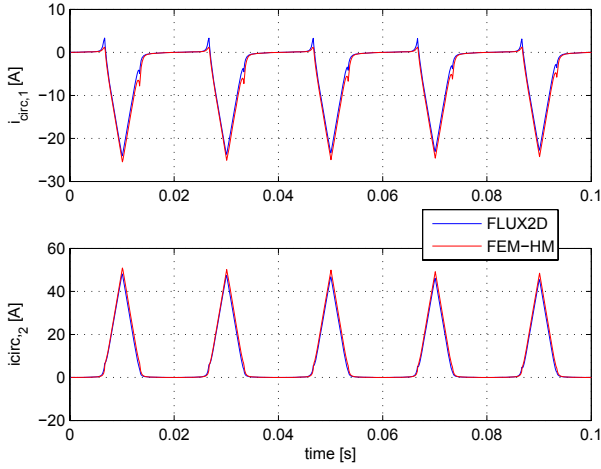
Fig. 5.5. Primary currents, switch on with square wave feed, open secondary.

5.3.2 Square wave feed

The general shape of the curves obtained with FEM-HM is correct. The error is greater than the one obtained with the cosine feed. However, the maximum value of the error is observed when the value of the feed voltage changes. It should be noted that during these instants both software are probably imprecise. Furthermore, despite this error, the simulation carried out with FEM-HM remains stable.

6

Slide-band and periodic limit conditions

This chapter deals with the slide-band and the periodic limits conditions. These two features are treated in the same chapter as the implementation of the periodic limit conditions has to take into account the presence of the slide-band. This point will be made clear in (sect. 6.3.2). Furthermore both of these features can be validated on the same geometry.

Comparison of the vector potential, flux and induced voltage with the values computed by Flux2D will be made. As no currents are computed, no link is made with an external solver i.e., only the FE solver is used.

6.1 Geometry and circuit

The machine used in this chapter is shown on (fig. 6.1). It is not the modelling of a real machine, but rather a test case that has been made as simple as possible to draw. This explains the peculiar shape of the rotor, as well as the concentrated stator winding.

Figure (6.2) shows the accompanying circuit. The stator is kept open as no current will be computed. Consequently, the equations
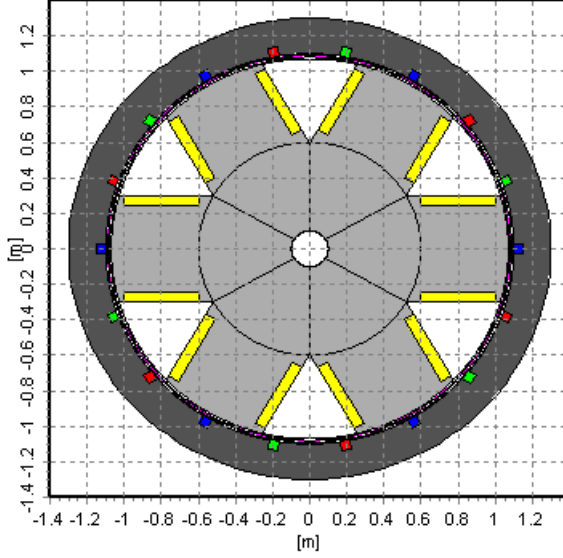
Fig. 6.1. Simple synchronous machine, test case.

solved are: the discretized Ampere's equations (6.1) and the expression yielding the induced voltage from the vector potential (6.2).

An expression for the flux is obtained by dropping the time derivative from (6.2).

$$M(\mu) \cdot \begin{bmatrix} A_1 \\ \vdots \\ A_n \end{bmatrix} = N \cdot i_f \tag{6.1}$$

$$T \cdot \frac{d}{dt} \begin{bmatrix} A_1 \\ \vdots \\ A_n \end{bmatrix} = \begin{bmatrix} u_{ind,1} \\ u_{ind,2} \\ u_{ind,3} \end{bmatrix} \tag{6.2}$$
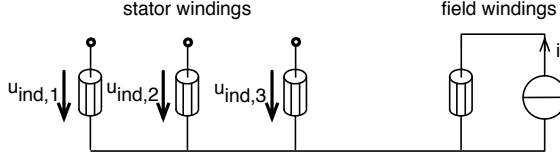
Fig. 6.2. Circuit.

6.2 Slide-band

6.2.1 Movement equation

Even if the simulations in this work are made at a constant speed, it is necessary to outline the resolution of the movement equation as to better understand how the rotation of the rotor will be taken into account.

The chosen method uses a separate solver for the movement equation (6.3),where I is the moment of inertia, α the angular position of the rotor and k_{tot} is the sum of the torques acting on the rotor. More precisely $k_{tot} = k_{em} + k_{frict} + k_{ext}$. Where k_{em}, k_{frict} and k_{ext} are respectively the electromagnetic, frictional and turbine or pump torque respectively.

$$k_{tot} = I \frac{d^2\alpha}{dt^2} \tag{6.3}$$

The FE and movement equations are then solved one after the other. After the FE problem and the linked circuit have been solved, a value for the torque is computed. This value is used to solve the movement equation, which yields the new speed of the rotor. The new position of the rotor is updated accordingly and a new FE and circuit resolution can begin (fig. 6.3).
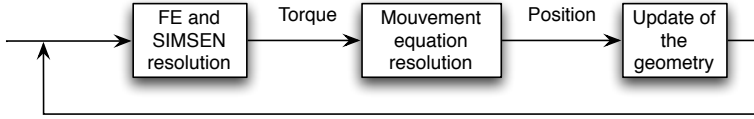
Fig. 6.3. Computation of a new position.

6.2.2 Dealing with a moving geometry

As said in (sect. 2.2.5), the slide-band is a layer of elements between the mesh of the rotor and the mesh of the stator which is re-meshed at each time step so as to enable the movement of the rotor.

The reference [37] shows that the error on the flux density in the air gap will directly influence the quality of the computed torque. Hence it is necessary to keep the elements in the airgap small and of good quality (sect. 2.2.2).

Therefore, when the rotor moves, it is important to ensure that the elements always have the optimal shape. For example in (fig. 6.4) starting with the configuration n°1, the rotor moves to the right and the slide-band mesh gets in the configuration n°2. At this point it is necessary to re-mesh the slide band as the optimal mesh is n°2'.

6.2.3 Simulation on the whole machine

The routines implementing a correct re-meshing of the slide band have been validated by comparing the flux (fig. 6.5) and induced voltage (fig. 6.6) in the stator as computed by FEM-HM and Flux2d. In both cases the curves of Flux2D and FEM-HM are perfectly identical. A near perfect agreement is expected, for two reasons: first the equations (6.1) are linear as only linear materials were used. Then (6.2) is in fact algebraic. The time derivative in (6.2) is only used to compute the induced voltages and, as no current is computed, the precision on these values at any given time step does not influence the precision of the following steps.
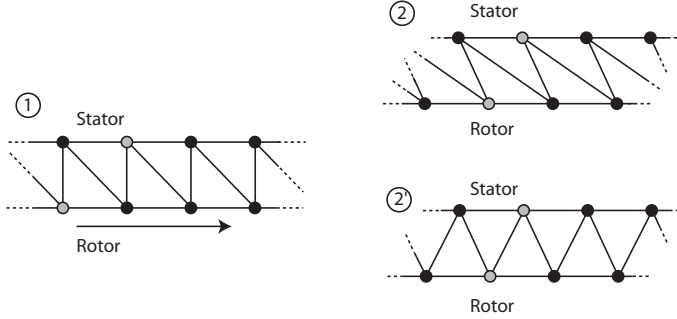
Fig. 6.4. Re-meshing of the slide-band.

The peculiar shape of the induced voltage (fig. 6.6) would not be acceptable for a real machine. However, it allowed an easier comparison between the curve of Flux2D and FEM-HM.

6.3 Periodic and anti-periodic limit conditions

The goal of this section is to present the theory required to understand the challenge of dealing with both periodic boundary conditions and a slide-band.

To simplify the text, the expression 'binary boundary' will be used when referred indifferently to a periodic or anti-periodic boundary condition.

The binary boundary conditions introduce a relationship between the value of the vector potential of two groups of nodes. This is illustrated by fig (6.7), which shows the same geometry than (fig. 6.1), albeit reduced to a single pole through the use of periodicities. On the reduced geometry, six nodes on the border carrying binary conditions are highlighted. The values of the potential at the nodes are linked by (6.4).
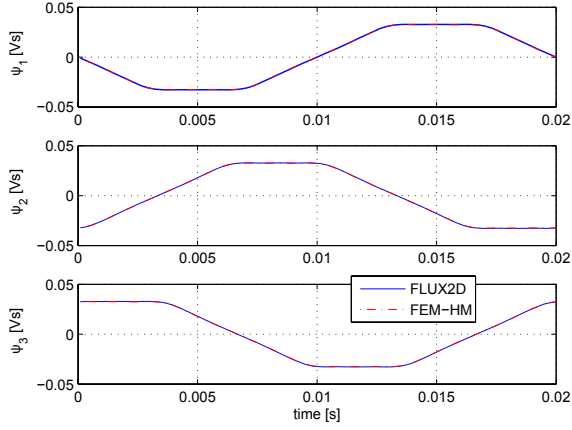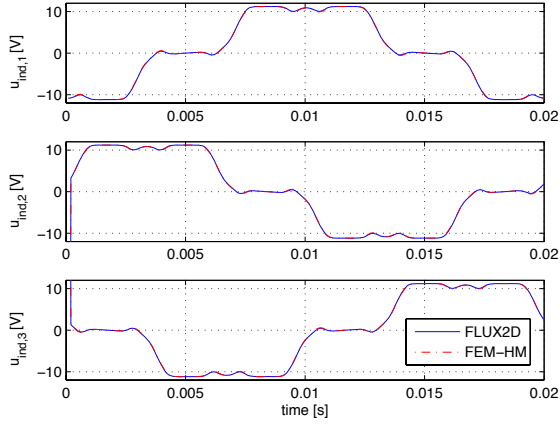
Fig. 6.5. Flux, whole geometry.

Fig. 6.6. Induced voltage, whole geometry.

$$A_1 = kA_4, \quad A_2 = kA_5, \quad A_3 = kA_6 \tag{6.4}$$

In the case of (fig. 6.7) an anti- periodic limit condition is used, the value of the nodes on the green line is thus the opposite of the value of the potential on the yellow line, ($k = -1$). The nodes on the yellow line are called reference, or free nodes, whereas the ones on the green line are called linked nodes. Which group of nodes is the reference and which is linked is, of course, arbitrary. In the case of periodic boundary conditions, the same definition holds with $k = 1$.

The addition of binary conditions will modify the matrix M and K from the discretized Ampere's equation (3.16 and 3.22), as well as the matrices T and C used to compute the induced voltages (3.20) and currents (3.24), respectively.

The next section will detail the modification to the matrix M needed to take the binary conditions into account. The principle is generalisable for the other matrices.

6.3.1 Building the matrix

The actual derivation of the expression for the entries of M has been treated in extenso by countless texts, cf. [24] and [38]. The entries of the matrix M are given by (6.5).

$$M_{ij} = \sum_E \iint_{s^{(e)}} \frac{1}{\mu^{(e)}} \nabla \alpha_i^{(e)} \nabla \alpha_j^{(e)} ds \tag{6.5}$$

Where the superscript $^{(e)}$ denotes the elements e and the subscripts $_{i,j}$ denotes the nodes i and j of element e. $\alpha_i^{(e)}$ is therefore the form function of node i defined on element e.

A short description of the data structure is needed. From an implementation point of view the mesh is described by a list of elements.

Each elements knows:

- the region it is part of;

- the nodes it is built on

  In turn each node knows:

- its coordinates;
- its vector potential;
- whether or not it is part of a boundary condition;
- if it is part of a periodic condition, the free node to which it is linked;
- if it is not part of a boundary condition, the index of the variable it defines

For a geometry without binary boundary the matrix M is built by going through the elements list. Then for each node pair on an element the contribution of theses nodes on this element is computed by (6.5) and added to the relevant entry of M. The only exception to this rule occurs when Dirichlet conditions are encountered. In this case, no contribution is computed as only homogeneous Dirichlet conditions are taken into account.

To assemble M on a geometry which has been reduced using binary conditions, the procedure is basically the same. However, the following special cases have to be taken into account.

One of the node is on a binary boundary:

- the contribution of the pair of nodes is computed in the usual way by (6.5);
- it is multiplicated by the factor k;
- it is then added to the entry defined by the free node and the node to which the node on the boundary is linked

Both nodes are on a binary boundary:

- the contribution of the pair of nodes is computed in the usual way (6.5);
- it is multiplicated by the factor $k_1 \cdot k_2$;
- it is added to the entry defined by the nodes to which the nodes on the boundary are linked

In this latter case k_1 and k_2 are the factors k of each of the binary conditions.

6.3.2 Adding the slide-band

While working on a reduced geometry there are two ways of dealing with the slide-band. The first one uses only the nodes present on (fig. 6.7). The second one uses a reduced geometry but a full slide-band (fig. 6.10 and 6.7).

For the first method, after each rotation the kind of binary conditions used on the slide-band is updated e.g., on (fig 6.10) when the rotor is in the position 1, all the nodes on its upper boundary belong to a periodic boundary condition, whereas in position 2, half of them are on a periodic boundary, and the other half are on anti-periodic conditions.

A peculiar case arises when the rotor is in front of the section of the stator which is actually modelled (fig. 6.7). In this case, periodic conditions are defined on the rotor, even if they are at the same location than the nodes they are linked to.

In the second method, the whole slide-band is kept. The innermost nodes are rotated with the rotor, while the outermost ones stay put. Each side of the slide-band holds binary conditions. The reference of the outermost nodes are the nodes directly in front of the stator, while for the innermost ones they are the nodes in front of the rotor. The figures (6.8) and (6.9) show the configuration of periodic and anti-periodic conditions used when a single pole, respectively a pair of poles is modelled. These configurations can be generalised to the case when any even (fig. 6.8), or odd (fig. 6.9) number of poles is used.

Assembling the matrix M when the second method is used also leads to problems. The assembling algorithm outlined in (sect. 6.3.1) works if all parts of the reduced geometry represent the same fraction of the original geometry. If the rotor and stator are reduced, but the slide band is complete (fig. 6.8) and (fig. 6.9), the contribution of the slide-band will be computed on the reference nodes and added

to the relevant entries of M. However the contributions from the linked nodes of the slide-band will also be added to the entries of the corresponding reference nodes. Therefore these entries will be three times too big in the case of (fig. 6.8) and six times too big in the case of (fig. 6.9).

One solution would be to multiply the contribution from the slide-band by the inverse of the fraction of the represented geometry. A somewhat simpler solution can be deduced from (fig. 6.11). In the section 1 the elements of the slide-band are present a single time. Their full contribution is added to the relevant entries of M. The elements of section 2 are present two times, consequently their contributions are divided by two. Finally all the elements of section 3 are already represented by the elements of section 1 or 2 therefore their contribution is simply not added to M. The distinction between the different sections is based on the number of linked nodes in the pair being considered.

To sum up the method, the contribution of the elements of the slide-band are treated according to the rules in (Tab. 6.1).

Section	Criterion	Factor
1	no linked node	1
2	1 linked node	0.5
3	2 linked nodes	0

Table 6.1. Contribution to M from the slide-band.

The second method will be used. It is a little easier to implement, as the nature of the binary conditions carried by a node does not change during the simulation.
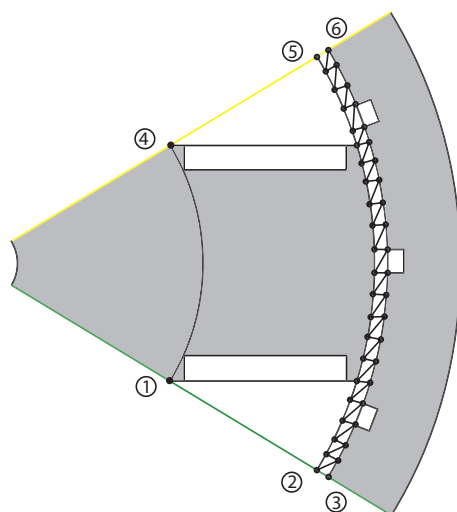
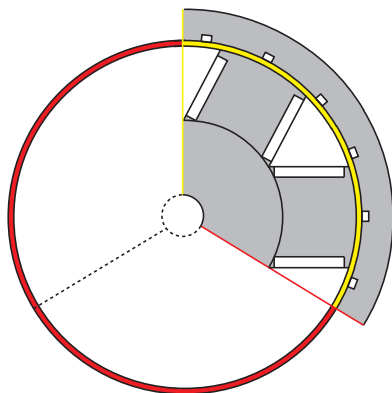**Fig. 6.7.** Reduced geometry of (fig. 6.1), reference nodes: yellow, inked nodes on anti-periodic condition: green.

Fig. 6.8. Boundary conditions, even number of poles modelled, reference nodes: yellow, linked nodes on periodic condition: red.
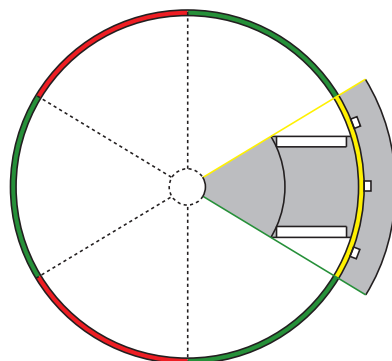

Fig. 6.9. Boundary conditions, odd number of poles modelled, reference nodes: yellow, linked nodes on anti-periodic condition: green, periodic condition: red.
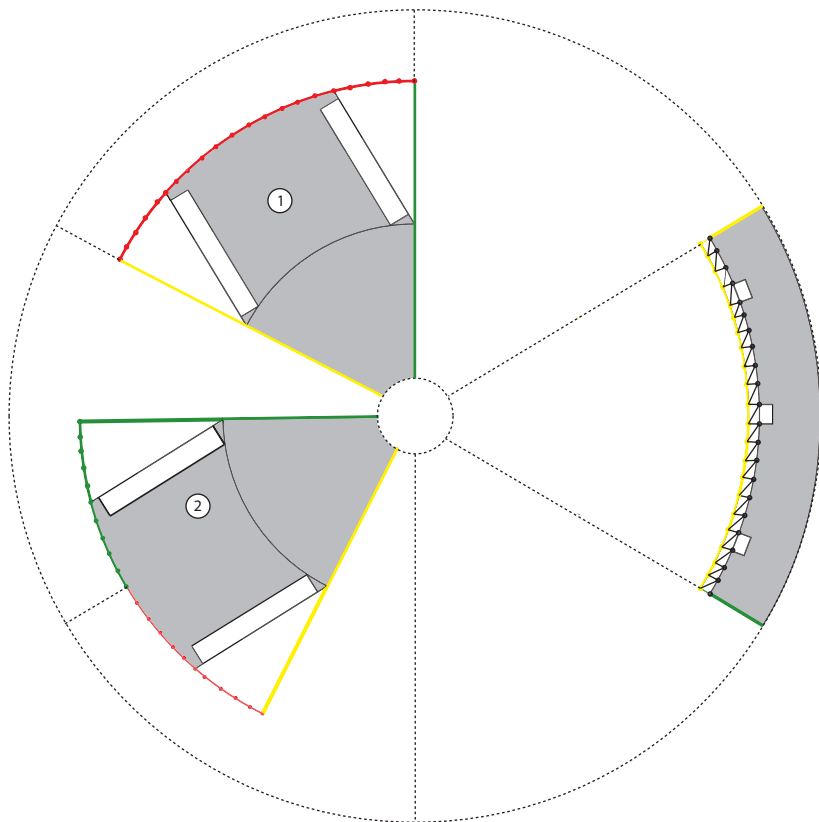
Fig. 6.10. Partial slide-band, the limit conditions change according to the position, reference nodes: yellow, linked nodes on anti-periodic condition: green, on periodic condition: red.
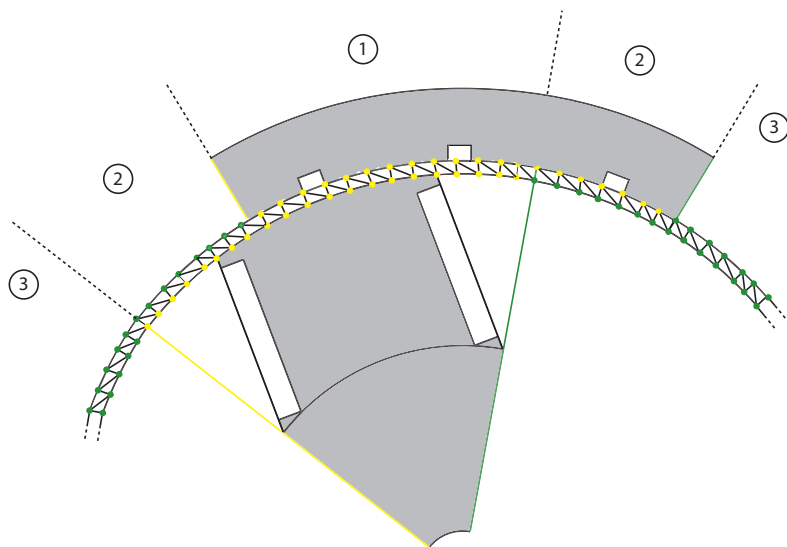
Fig. 6.11. Complete slide-band, dealing with the slide-band contribution.

6.3.3 Simulations on 1/6th of the machine

The first check was to ensure visually that the flux lines were correct in the reduced geometry. To this end, a current was applied to the field winding and a magneto-static simulation was performed. The flux lines are shown on (fig. 6.12).
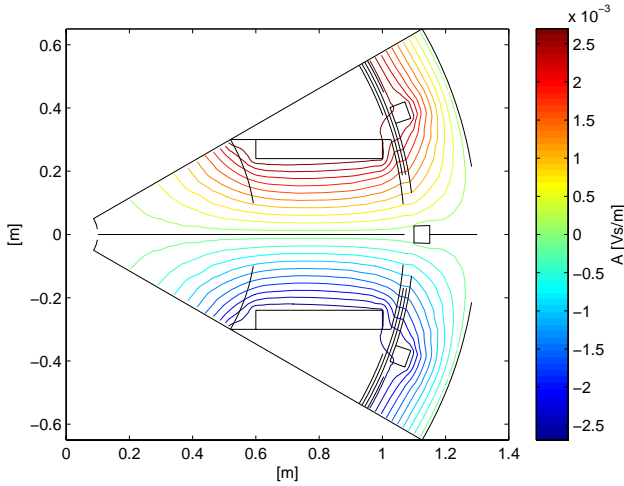

Fig. 6.12. Flux lines.

The next step was to check the value of the vector potential. The figure (6.13) shows the vector potential on the upper binary condition of (fig. 6.7), from the center of the machine axis to its periphery.

Finally the flux seen by the stator windings (ψ_1, ψ_2 and ψ_3) and the induced voltage were checked. They are shown on (fig. 6.14) and (fig. 6.15) respectively. The computed value of the flux and induced

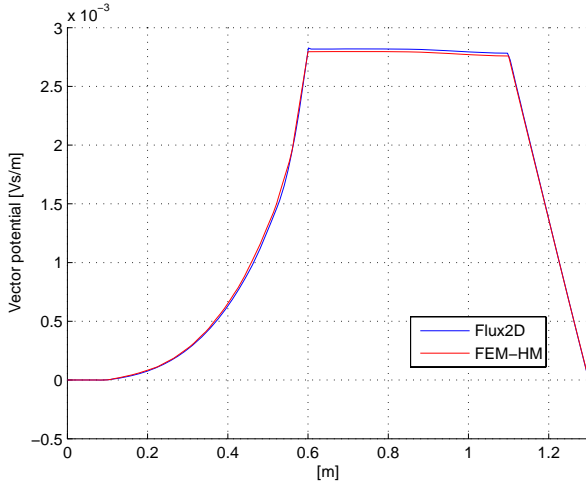voltage were multiplied by 6, to take into account the effect of the
whole machine.

Fig. 6.13. Vector potential on the upper boundary (from center to pe-
riphery) .

6.4 Conclusion

The need for the re-meshing of the slide-band has been outlined.
The implementation has been checked on a complete geometry by
computing both flux and induced voltages on a moving geometry.

Reducing a geometry using binary boundary conditions creates a
particular issue when a slide-band is also present. A simple method
dealing with this issue has been described. Its implementation has
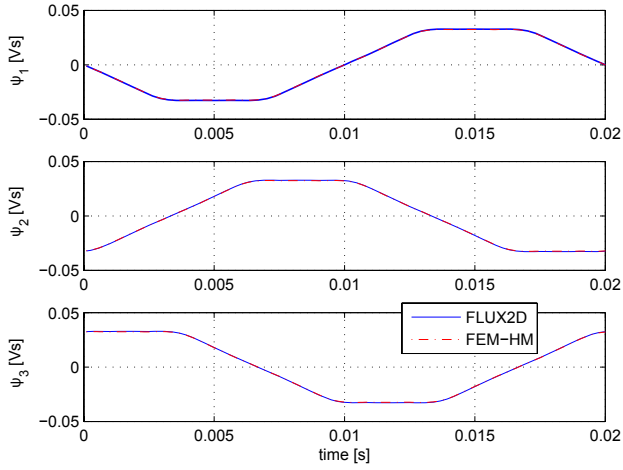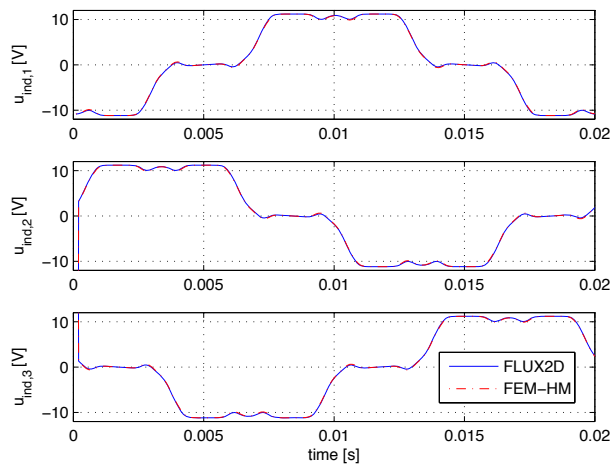been validated both at standstill and when the rotor is turning.

Fig. 6.14. Flux.

The next steps are, first the computation of currents and the link with an external solver. These two points will be checked in the next chapter by the simulation of an induction machine fed by a sine network. This machine will also be made of saturable iron.

Fig. 6.15. Induced voltage.

7

Induction Machine

This chapter presents the modelling of a squirrel cage induction machine. The goals are to test the implementation of the squirrel cage circuit and the computation of the torque. The robustness of the linking method is also tested.

It should be noted that this is an important step towards the simulation of the synchronous machine, as the squirrel cage of the induction machine and the damper cage of the synchronous machine are essentially the same device.

The solvers and communication methods used here are the same than in the example of the single-phase transformer (sect. 4.1.4). The feed cicruit is solved by the Runge-Kutta 4 method, the FE equations along with the accompanying circuit by the backward Euler method and they are both linked with the method described in (sect. 3.7.3).

7.1 Machine and FE modelling

The machine studied in this chapter is a small 7.5 [kW], squirrel cage induction machine, described in [39]. It has 2 poles and its rated voltage is 660[V]. Its geometry is shown on (fig. 7.1, 7.2). As it is apparent on the former picture, the complete geometry was

simulated. The stator has a diameter of 212 [mm] and the length of the magnetic core is 125 [mm]. Its cage is made of 20 bars.
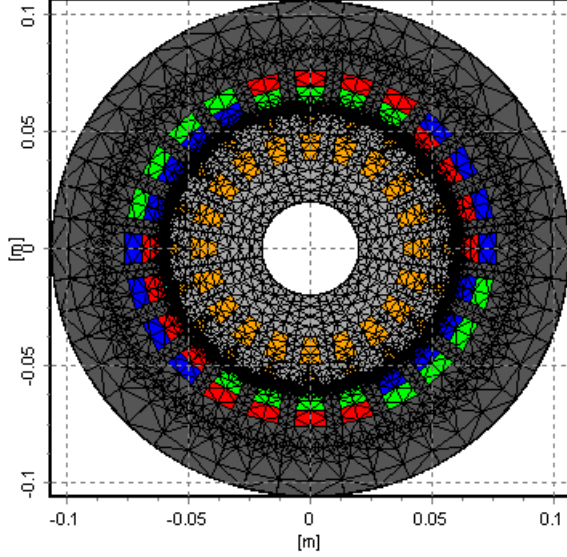

Fig. 7.1. Induction machine geometry.

7.2 Circuit of the squirrel cage

The damper cage is modelled by the standard ladder circuit shown on (fig. 7.3). As said in (sect. 2.2.3) the short-circuit ring influence is taken into account by the additional inductance ($L_{b,k}$, $L_{t,k}$) and resistance ($R_{b,k}$, $R_{t,k}$) connecting the bars (fig. 7.4).

Switches have been added in series with the bars. They allow to set the current in the bars to 0, which is useful to get the steady-
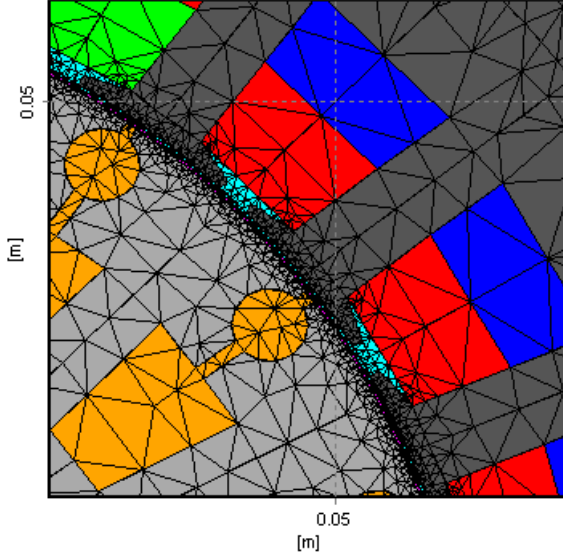
Fig. 7.2. Induction machine, bar zoomed.

state quickly when starting from null initial conditions. Their use is further described in (sect. 8.5.2).

7.2.1 Number of unknown

The chosen unknown are the branch currents. It is obvious from (fig. 7.4) that each additional bar adds three currents to the set of unknown i.e., one in the bar itself and one in each of the short-circuit ring connecting the bar to its neighbour. There is therefore $3 \cdot n_b$ unknown, where n_b is the number of bars in the cage.

Each additional bar adds two nodes to the circuit, therefore there is $2 \cdot n_b - 1$ independent current equations. As the circuit comprises $3 \cdot n_b$ branches and $2 \cdot n_b$ nodes, it has $3 \cdot n_b - 2 \cdot n_b + 1$ independent voltage equations (cf. [40] p110).
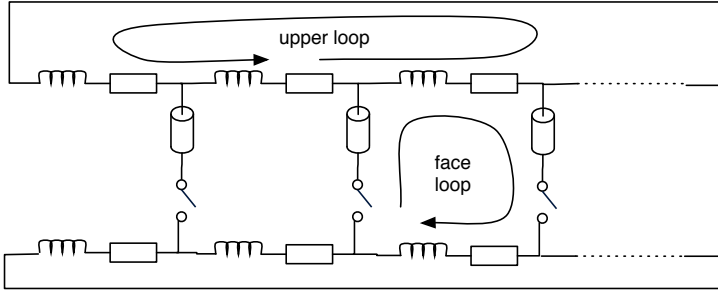
Fig. 7.3. Circuit of a damper cage.

7.2.2 Nomenclature

The name of the variables and components relative to the k-th bar are explained on (fig. 7.4). To differentiate between the variables and components of the upper and lower short-circuit ring, they are marked with the subscript t for top and b for bottom respectively. For the same reason the variables in the branch of the bars are marked with the subscript v for vertical.

7.2.3 Current equations

The equations for the k-th bar are (7.1) and (7.2) for the upper and lower nodes respectively. This holds for every bar but the first, hence $k \in [2; n_b]$. It has been decided to drop the equation related to the lower node of the first bar, in consequence the contribution of the first bar is reduced to (7.3).

$$0 = i_{t,k-1} - i_{t,k} - i_{v,k} \tag{7.1}$$

$$0 = i_{v,k} + i_{b,k} - i_{b,k-1} \tag{7.2}$$
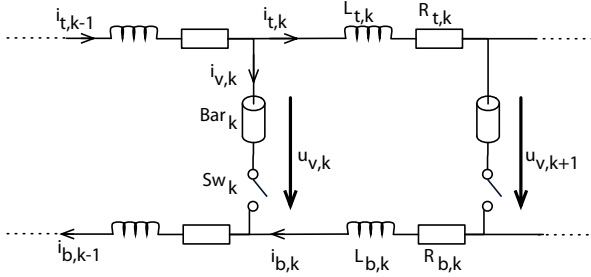
Fig. 7.4. k-th bar.

$$0 = -i_{t,1} - i_{v,1} + i_{t,nb} \tag{7.3}$$

7.2.4 Voltage equations

The loops chosen to establish the voltage equations are the ones made of two consecutive bars 'face loops' and the one running along the upper short-circuit ring 'upper loop' cf. (fig. 7.3).

For all the bars but the last one, the equation related to the 'face loop' is (7.4), with $k \in [1; n_b - 1]$. The equation related to the last bar is (7.5), and the one of the upper short-circuit ring is (7.6).

$$0 = -u_{v,k} + R_{t,k} \cdot i_{t,k} + L_{t,k} \cdot \frac{di_{t,k}}{dt} +$$
$$u_{v,k+1} + R_{b,k} \cdot i_{b,k} + L_{b,k} \cdot \frac{di_{b,k}}{dt} \tag{7.4}$$

$$0 = -u_{v,nb} + R_{t,nb} \cdot i_{t,nb} + L_{t,nb} \cdot \frac{di_{t,nb}}{dt} +$$
$$u_{v,1} + R_{b,nb} \cdot i_{b,nb} + L_{b,nb} \cdot \frac{di_{b,nb}}{dt} \tag{7.5}$$

$$0 = \sum_{k=1}^{n} \left(R_{t,k} \cdot i_{t,k} + L_{t,k} \cdot \frac{di_{t,k}}{dt} \right) \qquad (7.6)$$

Finally, the total voltage on the bar and the switch $u_{v,k}$ is given by (7.7), where $R_{sw,k}$ and $L_{sw,k}$ are respectively the resistance and inductance of the k-th switch. The voltage $u_{bar,k}$ is the voltage on the bar itself. It is computed separately by (7.8) as it is the source term for the bars on the FE side. In this latter equation $R_{bar,k}$ is the resistance of the bar and $i_{ind,k}$ the induced current, which is computed by (3.24).

$$u_{v,k} = u_{bar,k} + R_{sw,k}i_{v,k} + L_{sw,k}\frac{di_{v,k}}{dt} \qquad (7.7)$$

$$u_{bar,k} = R_{bar,k}(i_{v,k} - i_{ind,k}) \qquad (7.8)$$

7.3 Stator circuit

The circuit of the stator is the same as the one of the primary windings of the three-phases transformer (ch. 5.2). In consequence it will not be described here.

7.4 Complete equations set

The complete equations set is made of the FE equations (7.9), the definition of the induced voltages in the windings (7.10), the induced currents in the bars (7.11), the circuit equations of the cage (7.1)-(7.8) and the ones of the stator windings. These later equations are the same as the equations of the primary windings of the three-phases transformer (5.1) and (5.4). They will not be repeated here.

$$K \cdot \frac{d}{dt} \begin{bmatrix} A_1 \\ \vdots \\ A_n \end{bmatrix} + M(\mu) \cdot \begin{bmatrix} A_1 \\ \vdots \\ A_n \end{bmatrix} = \begin{bmatrix} S \\ \hline N \end{bmatrix} \cdot \begin{bmatrix} u_{bar,1} \\ \vdots \\ u_{bar,20} \\ \hline i_{fem,1} \\ i_{fem,2} \\ -i_{fem,1} - i_{fem,2} \end{bmatrix} \qquad (7.9)$$

$$\begin{bmatrix} u_{ind,1} \\ u_{ind,2} \\ u_{ind,3} \end{bmatrix} = T \cdot \frac{d}{dt} \begin{bmatrix} A_1 \\ \vdots \\ A_n \end{bmatrix} \qquad (7.10)$$

$$\begin{bmatrix} i_{ind,1} \\ \vdots \\ i_{ind,20} \end{bmatrix} = C \cdot \frac{d}{dt} \begin{bmatrix} A_1 \\ \vdots \\ A_n \end{bmatrix} \qquad (7.11)$$

7.5 Computation of the torque

The torque k_{em} is computed using Maxwell's stress tensor [36]. A full derivation of the method used is available in [37]. This method yields the torque through a simple line integral along the middle of the slide-band(7.12),

$$k_{em} = \frac{1}{\mu_0} hr \int_l B_r B_\theta dl \qquad (7.12)$$

where B_θ and B_r are respectively the tangential and radial component of the flux density, r is the radius of the middle of the slide-band and h is the equivalent depth of the model. The integral is calculated on the path shown on (fig. 7.5).
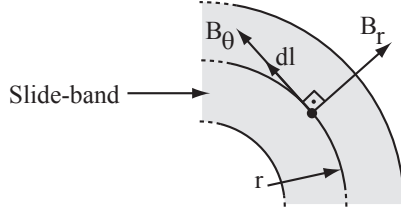
Fig. 7.5. Integral for the computation of the torque.

7.6 Simulations and results

Two different kind of simulations are carried out. The first one is a switch-on at constant speed, starting with null initial conditions. The goal is to check the implementation of the damper cage circuit and of the torque computation.

Two of these simulations are presented here. The first one with a slow speed (s= 0.9), the second one close to the synchronous speed (s= 0.05).

The second kind of simulation is a short-circuit from a steady-state operating point. The goal is to further check the robustness of the linking method when the feed voltage changes abruptly. This simulation has two parts: the currents stabilization part from $t = 0$ to the short-circuit at $t = 60[ms]$, and the short-circuit part afterwards.

To shorten the time needed for the currents to stabilize, the values of the resistors in the accompanying and feed circuit (R_{circ}, R_{fem}, $R_{t,k}$, $R_{b,k}$ and $R_{bar,k}$) are 20 times greater than their real values during the first part of this simulation. At the instant of the short-circuit they are restored to their real values.

For each of these simulations the stator currents, three bar currents and the torque are shown here. The bars, whose current are represented, are shown on (fig. 7.6).
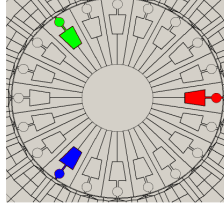
Fig. 7.6. Bar number: red 1, green 8, blue 14.

The results are presented in the next sections. The stator, bars currents and torque obtained during the switch-on with $s = 0.05$ are shown on (fig. 7.7), (fig. 7.8) and (fig. 7.9) respectively.

For the simulation with $s = 0.9$ they are presented on (fig. 7.10), (fig. 7.11) and (fig. 7.12). The error between the values obtained with Flux2D and FEM-HM are summed up in (tab. 7.1) and (tab. 7.2).

For the short-circuit the stator, bars currents and torque are shown on (fig. 7.13), (fig. 7.14) and (fig. 7.15). The error between Flux2D and FEM-Hm are in (tab. 7.3).
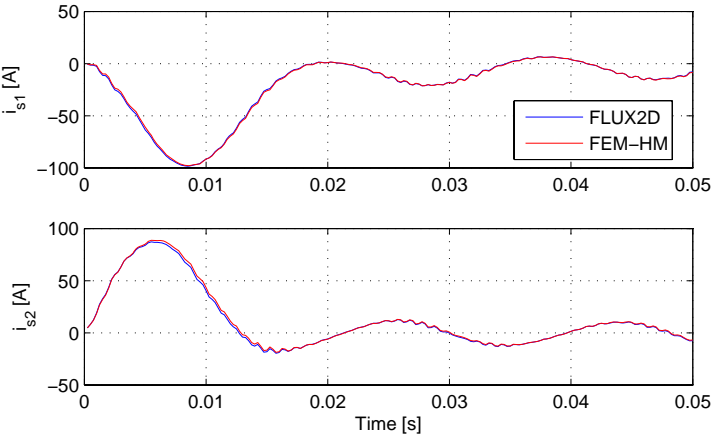
7.6.1 Constant speed (slip, $s = 0.05$), switch-on

Fig. 7.7. Stator currents, $s = 0.05$.

i_{s1}	i_{s2}	i_{b1}	i_{b8}	i_{b14}	Torque
2.3 %	3.7 %	3.6 %	7.1 %	4.8 %	6.5 %

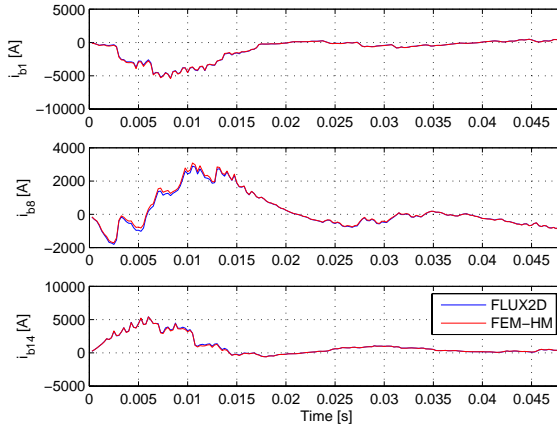**Table 7.1.** Maximal error between Flux2D and FEM-HM, s= 0.05.

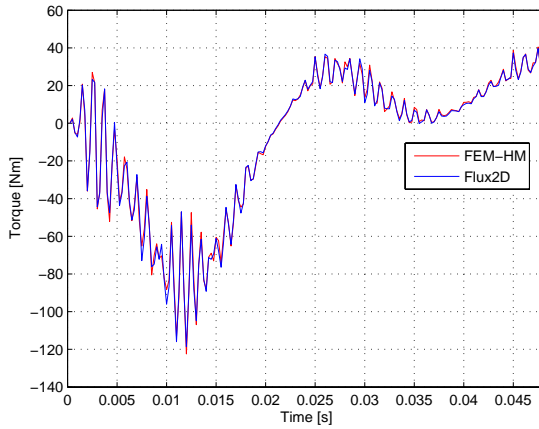**Fig. 7.8.** Bars currents, $s = 0.05$.

Fig. 7.9. Torque, $s = 0.05$.

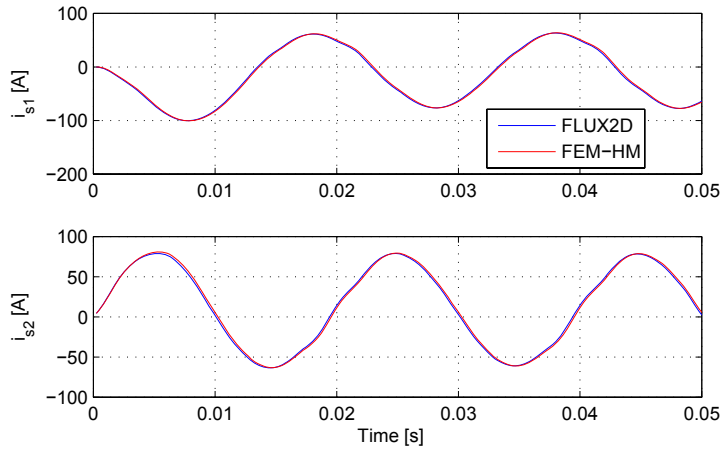**Constant speed (slip, $s = 0.9$), switch-on**

Fig. 7.10. Stator currents, $s = 0.9$.

i_{s1}	i_{s2}	i_{b1}	i_{b8}	i_{b14}	Torque
3.9 %	5.0 %	6.2 %	5.5 %	6.6 %	6.5 %

Table 7.2. Maximal error between Flux2D and FEM-HM, s= 0.9.
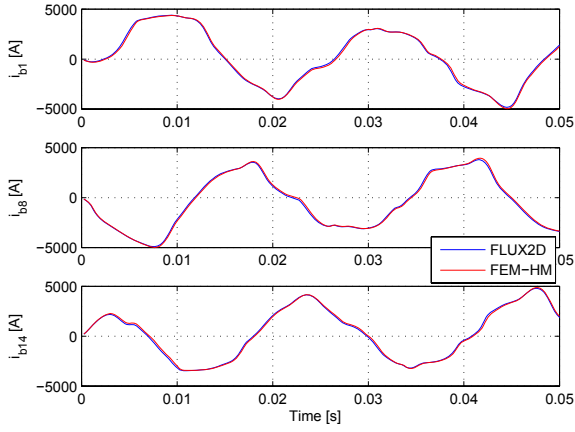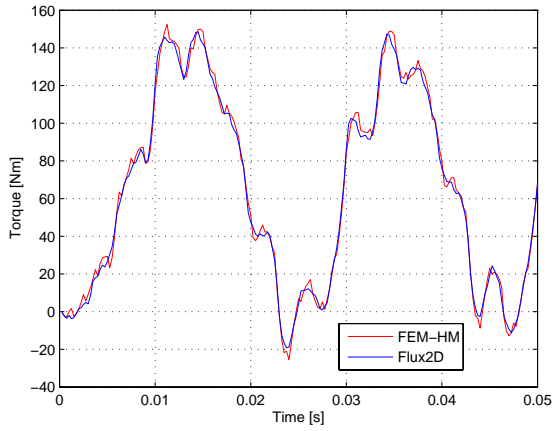
Fig. 7.11. Bars currents, $s = 0.9$.

Fig. 7.12. Torque, $s = 0.9$.

7.6.2 Short-circuit
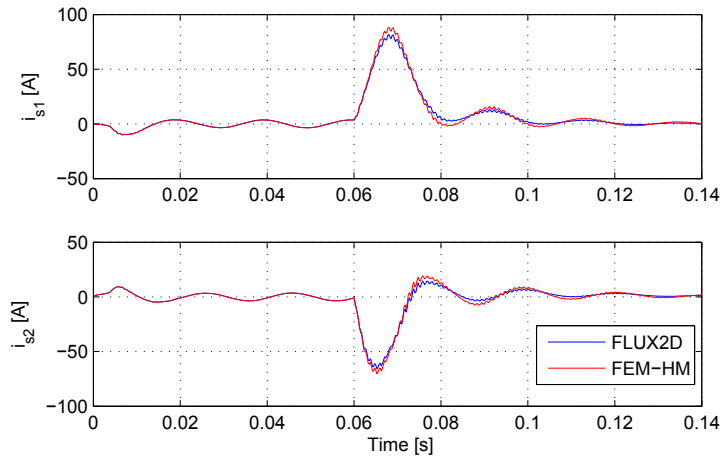

Fig. 7.13. Stator currents, short-circuit.

i_{s1}	i_{s2}	i_{b1}	i_{b8}	i_{b14}	Torque
8.3 %	9.3 %	7.0 %	10 %	8.5%	8.7 %

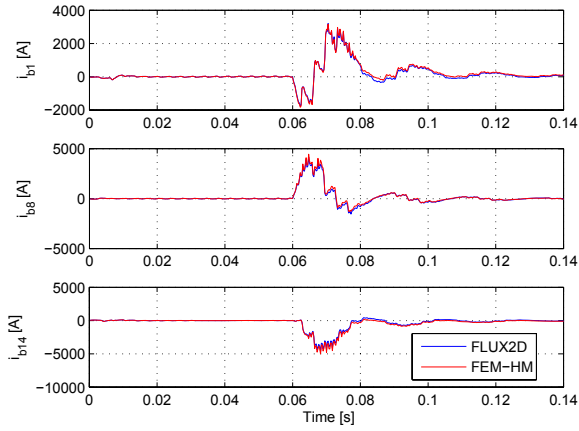**Table 7.3.** Maximal error between Flux2D and FEM-HM, short-circuit.

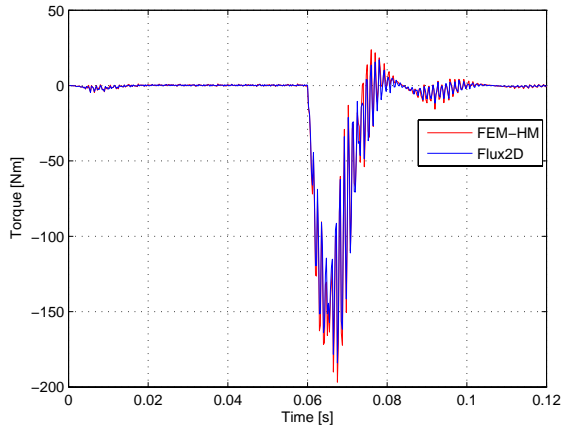**Fig. 7.14.** Bars currents, short-circuit.

Fig. 7.15. Torque, short-circuit.

7.7 Conclusion

There are three goals for this chapter. The first one is to validate the implementation of the damper cage. The second is to provide a first test of the torque computation. Finally the short-circuit provides a further test of the robustness of the linking method.

The good concordance between the currents computed by FEM-HM and Flux2D shows that the implementation of the damper cage is correct.

The error on the torque is not greater than the error on the currents. This proves that the routine computing the torque has been correctly implemented.

Lastly, the error on the short-circuit simulation is greater than the one observed during the switch-on. This is similar to what had been observed on the example of the three-phases transformer where the simulation with a sinusoidal feed bears a smaller error than the one with a square wave feed.

8

Hydro generator

The machine modelled in this chapter is a 83 [MVA] salient pole hydro generator with full damper cage. It has 5 pairs of poles ($2p = 10$) and its nominal voltage is 17 500 [V]. All the necessary documentation for its modelling has been provided by its manufacturer.

Two simulations are carried out. First, the unloaded induced voltage predicted by the model is checked. This is mainly to ensure that the FE model itself is correct. Then a two phases short-circuit is simulated. In the former case no currents are computed and only the FE solver is used. It is the same situation as for the simple synchronous machine of (ch. 6). In the latter case the solver and communication method used are, once again, the same than the one described in (sect. 4.1.4).

8.1 Geometry

The modelled machine has an integer number of slots by pole by phase (4, as is readily apparent from (fig. 8.1)), furthermore the poles shoes are symmetrical. It is Therefore sufficient to take a single pole into account for the FE modelling. In consequence anti-periodic

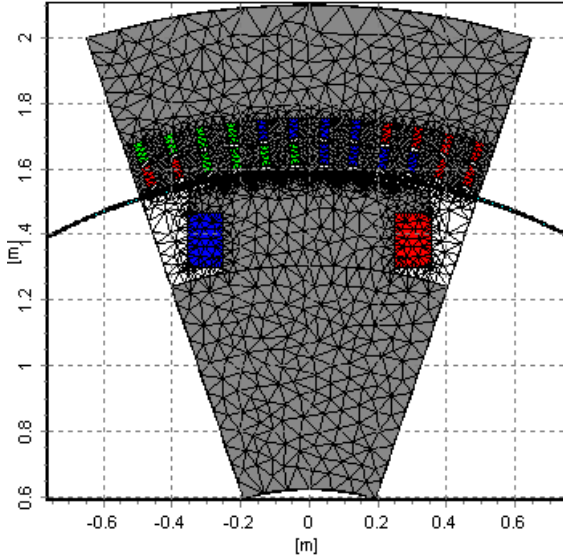boundary conditions are used, in the configuration represented in
(fig. 6.9).

Fig. 8.1. Hydro generator, geometry.

8.2 Damper cage with partial geometry

Before dealing with the circuit of the hydro generators it is necessary
to examine how to handle the damper cage when the geometry has
been reduced using anti-periodic boundary conditions. To this end
the example of a two poles machine with a full damper cage made of
6 bars will be treated. Its rotor is represented on (fig. 8.3) and the
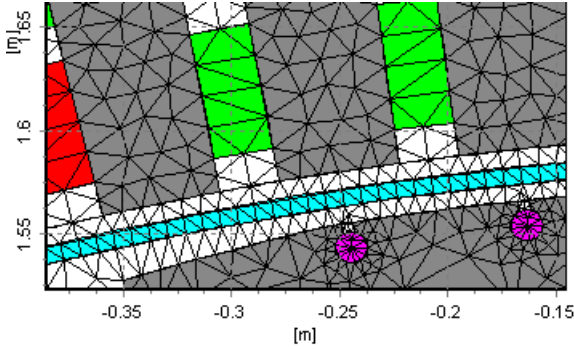cage circuit on (fig. 8.4).

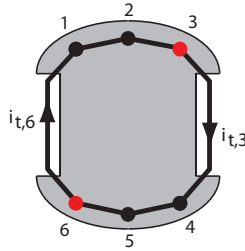**Fig. 8.2.** Hydro generator, mesh in the air-gap.

Fig. 8.3. Rotor with a six bars damper cage.

The reduced model will be made of the upper pole only. The circuit is similarly cut i.e., only the components on the left half of the circuit are kept. This leaves the currents $i_{t,6}$, $i_{t,3}$, $i_{b,3}$ and $i_{b,6}$ dangling. The goal is to find a way to reconnect them so that every current and voltage in the reduced circuit have the same value as in the complete circuit.

Since anti-periodic boundary conditions are used, it follows that two variables 180°apart are the opposite one of the other. Hence, the electrical variables of the cage are linked by (8.1) to (8.3).
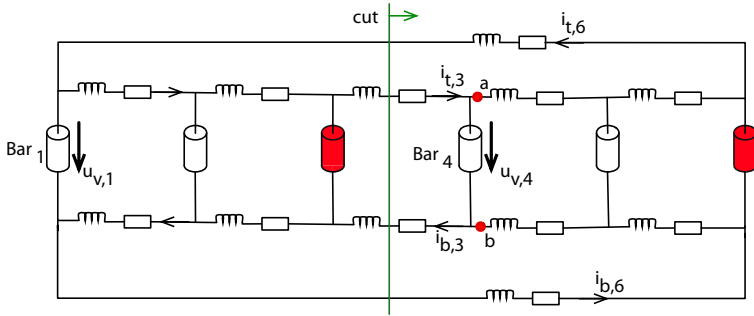
Fig. 8.4. Six bars damper cage circuit.

$$u_{v,1} = -u_{v,4} \tag{8.1}$$

$$i_{t,3} = -i_{t,6} \tag{8.2}$$

$$i_{b,3} = -i_{b,6} \tag{8.3}$$

The goal is to define $(i_{t,3})$ and $(i_{b,3})$ without using the variable from the second half of the machine. To this end the cut equation (8.4)is written. The position and direction of the cut is indicated on (fig. 8.4).

$$0 = -i_{t,6} + i_{t,3} - i_{b,3} + i_{b,6} \tag{8.4}$$

By substituting either $i_{t,6}$ and $i_{b,3}$ or $i_{t,3}$ and $i_{b,6}$ in (8.4), it yields (8.5) and (8.6). It is therefore possible to connect the limbs carrying the currents $i_{b,6}$ and $i_{t,3}$ respectively $i_{b,3}$ and $i_{t,6}$. The circuit thus reduced is shown on (fig. 8.5). It should be noted that these added connections impose $-u_{v,1} = u_{v,4}$.

$$i_{t,3} = i_{b,6} \qquad (8.5)$$
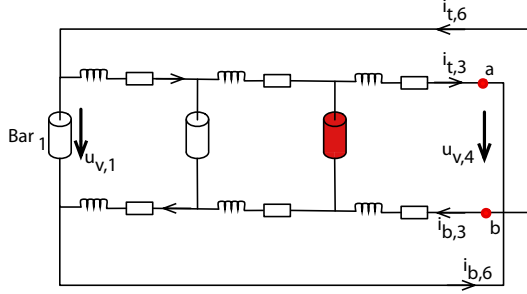
$$i_{b,3} = i_{t,6} \qquad (8.6)$$

Fig. 8.5. Six bars damper cage circuit, reduced by anti-periodic boundary conditions.

8.2.1 Equations for the reduced damper cage

The equations of the damper cage remain basically the same. Only the ones which depend on the first or last bar have to be modified. These modifications are highlighted in bold in the next paragraphs. As in the previous chapter, n_b is the number of bars present in the geometry.

Current equations

Here, only the equations of the first bar (7.3) have to be modified. The upper node of the first bar is now connected to the lower node of the last bar and thus this equation becomes (8.7)

$$0 = -i_{t,1} - i_{v,1} - \mathbf{i_{t,nb}} \qquad (8.7)$$

Voltage equations

The equation relative to the last 'face loop' (7.5) has to be updated, the first 'vertical' voltage is now counted negatively (8.8).

$$0 = -u_{v,nb} + R_{t,nb} \cdot i_{t,nb} + L_{t,nb} \cdot \frac{di_{t,nb}}{dt} +$$

$$-\mathbf{u_{v,1}} + R_{b,nb} \cdot i_{b,nb} + L_{b,nb} \cdot \frac{di_{b,nb}}{dt} \tag{8.8}$$

The equation relative to the 'upper loop' also has to be modified. To close the loop it is now also necessary to go through the bottom components (8.9).

$$0 = \sum_{k=1}^{n} \left(R_{t,k} \cdot i_{t,k} + L_{t,k} \cdot \frac{di_{t,k}}{dt} \right.$$

$$\left. -\mathbf{R_{b,k}} \cdot \mathbf{i_{b,k}} - \mathbf{L_{b,k}} \cdot \frac{\mathbf{di_{b,k}}}{\mathbf{dt}} \right) \tag{8.9}$$

8.3 Complete circuit of the hydro generator

The circuit of the hydro generator is made of the stator winding circuit, the field winding circuit and the damper cage circuit. The stator winding has the same circuit as the primary windings of the three-phases transformer. It is shown on (fig. 5.2).

The field winding circuit is shown on (fig. 8.6). It adds one intermediate voltage as the voltage across the field windings terminals is usually set by the grid solver.

The circuit of the damper cage is shown on (fig. 8.7). It is made of seven bars connected such as to take the anti-periodic boundary conditions into account.
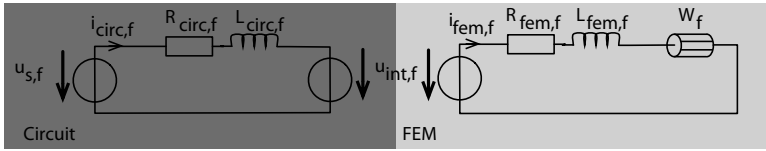
Fig. 8.6. Circuit of the field winding.
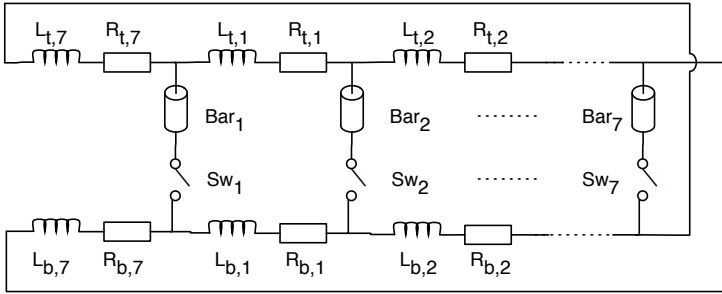
Fig. 8.7. Circuit of the damper cage.

8.4 Equations set

The complete equations set of the hydro generator model is made of the FE equations (8.10), the induced voltages and currents equations (8.11), (8.12), to which the stator winding equations (5.1) and the field winding equation (8.13) are added. The contribution of the damper cage are the currents equations (7.1), (7.2) and (8.7) and the voltages equations (7.4), (8.8) and (8.9).

$$
K \cdot \frac{d}{dt} \begin{bmatrix} A_1 \\ \vdots \\ A_n \end{bmatrix} + M(\mu) \cdot \begin{bmatrix} A_1 \\ \vdots \\ A_n \end{bmatrix} = \left[\begin{array}{c|c} S & \\ \hline & N \end{array} \right] \cdot \begin{bmatrix} u_{bar,1} \\ \vdots \\ u_{bar,7} \\ \hline i_{fem,1} \\ i_{fem,2} \\ -i_{fem,1} - i_{fem,2} \\ i_{fem,f} \end{bmatrix} \qquad (8.10)
$$

$$
\begin{bmatrix} u_{ind,1} \\ u_{ind,2} \\ u_{ind,3} \\ u_{ind,f} \end{bmatrix} = T \cdot \frac{d}{dt} \begin{bmatrix} A_1 \\ \vdots \\ A_n \end{bmatrix} \qquad (8.11)
$$

$$
\begin{bmatrix} i_{ind,1} \\ \vdots \\ i_{ind,7} \end{bmatrix} = C \cdot \frac{d}{dt} \begin{bmatrix} A_1 \\ \vdots \\ A_n \end{bmatrix} \qquad (8.12)
$$

$$
u_{int,f} = R_{fem,f} \cdot i_{fem,f} + L_{fem,f} \cdot \frac{di_{fem,f}}{dt} + u_{ind,f} \qquad (8.13)
$$

8.5 Simulation and results

Two simulations are presented here. The first aims to check the induced voltages under no-load operation. The second one is a two-phases short-circuit. As usual, the values obtained by FEM-HM are compared to the one obtained with Flux2D.

8.5.1 Induced voltage

The goal of this simulation is to check the FE model (boundary conditions, magnetic characteristics of the iron, slide-band) of the hydro generator. The quantity computed is the no-load voltage on steady-state operation.

As such, the rotor turns at nominal speed, the stator windings are left open and the rotor winding is fed by a current source, whose value is $i_{f0} = 621.1[A]$. In consequence, no windings currents are computed and no link is made with an external solver. Furthermore, the currents in the damper cage are neglected. The bars are replaced by air in the FE model.

The induced voltage on each of the stator winding are shown on (fig. 8.8). The curve from Flux2D and the one computed by FEM-HM are virtually identical, as was the case with the simple synchronous machine of (ch. 6).

The magnitude of the voltage is also consistent with the value given by the manufacturer. The peak value of the voltage computed here is $1382[V_p]$. This is a phase-to-neutral voltage computed on 1/10th of the machine, consequently the total phase-to-phase voltage is $1382 \cdot \sqrt{3}/\sqrt{2} \cdot 10 = 16\ 926[V_{rms}]$.

8.5.2 Two-phases short-circuit

This section gives a validation of the ability of FEM-HM to simulate a hydro generator in transient conditions.

Like the short-circuit of the induction machine this simulation is also made of two parts: an initialization and then the short-circuit itself. During the initialization stage the field winding is fed by a current source and the switches of the cage is left open. This is done for the following reason:

As null initial conditions are used, it means that at the first time step the flux seen by the windings and damper cage jumps from 0 to a non-null value. This quick variation of flux yields huge induced voltages. If the currents in the windings and damper cage were left free to vary they would have a correspondingly huge value and would take a long time to decay.

For this reason during the first 20 milliseconds of the simulation, the switches of the cage are left open. At the same time the circuit equations of the windings are taken out of the equations set and the
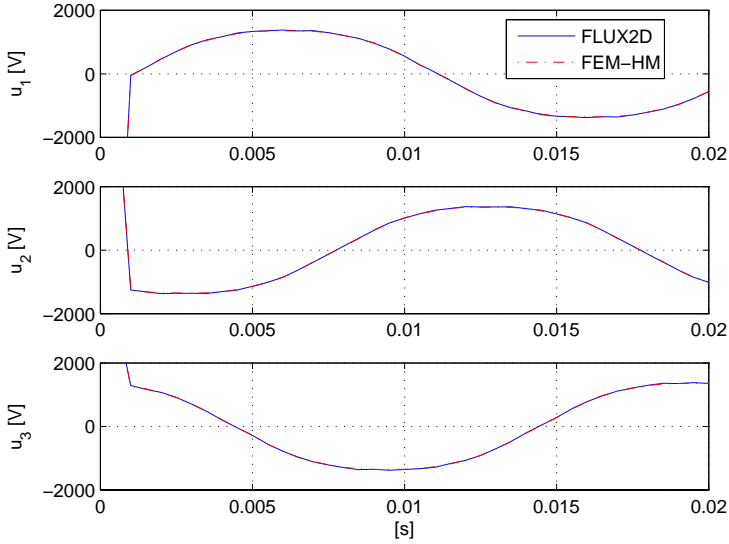
Fig. 8.8. Induced voltage.

value of the currents are set directly in (8.10), $i_{fem,1} = 0$, $i_{fem,2} = 0$ and $i_{fem,f} = i_{f0}$.

The initialization is performed by the FE solver only. At the instant of the short-circuit, the circuit equations are brought back and the link is restored. At the same time the currents of the feed circuit and the intermediate voltages are initialized according to the values computed by the FE solver.

After that a short-circuit between the phases 1 and 2 is simulated by setting $u_{s,1}$ to 0. The third phase is left open by setting $R_{circ,3} = 10^8 [\Omega]$ and $L_{circ,3} = 10^8$ [H].

Currents in the windings

As it can be expected the currents in the stator windings 1 and 2 (fig. 8.9) are the opposite of each other. The curves issue from FEM-HM closely follows the one from Flux2D. The values from FEM-HM are shifted compared to the ones from Flux2D. Their maximum values are however very close.

The curves of the field currents from FEM-HM and Flux2D are shown on (fig. 8.9). These curves are practically superposed. The maximal error on the windings currents are summed up in (tab. 8.1).

Stator winding 1	Stator winding 2	Field winding
7.4%	7.4%	2.8 %

Table 8.1. Error on the windings currents

Currents in the bars

The currents in the bars are shown on (fig. 8.11) to (fig. 8.17). The overall shape of the curves are similar. There is however a discrepancy on the maximum value of the currents. The maximal errors between the values computed by Flux2D and FEM-HM are summed up in (tab. 8.2).

Bar 1	Bar 2	Bar 3	Bar 4	Bar 5	Bar 6	Bar 7
29%	19%	15%	14%	12%	14%	27%

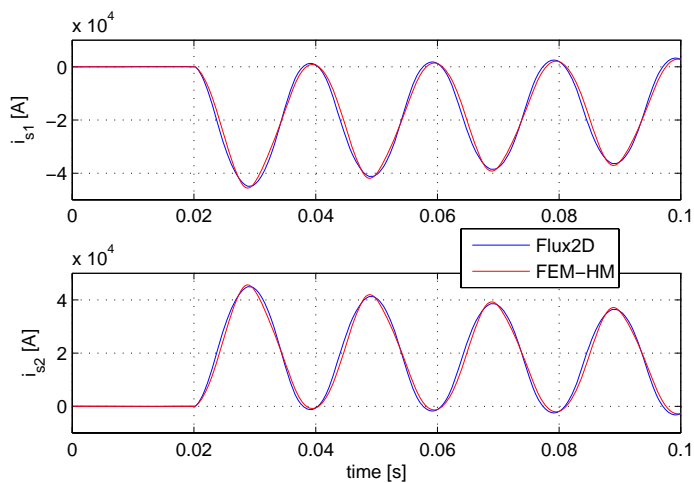**Table 8.2.** Error on the damper cage's bar currents

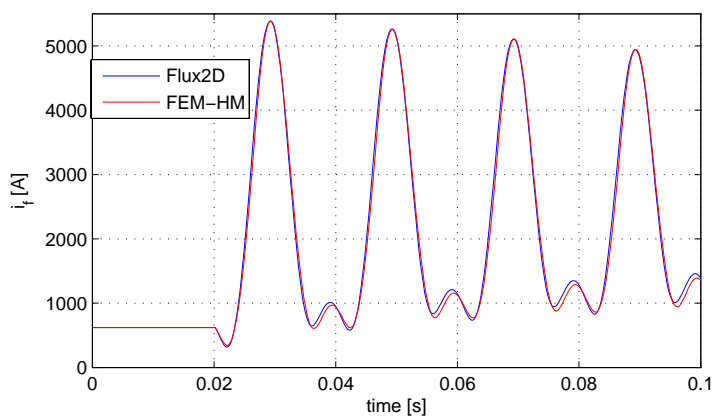**Fig. 8.9.** Currents in the stator windings.

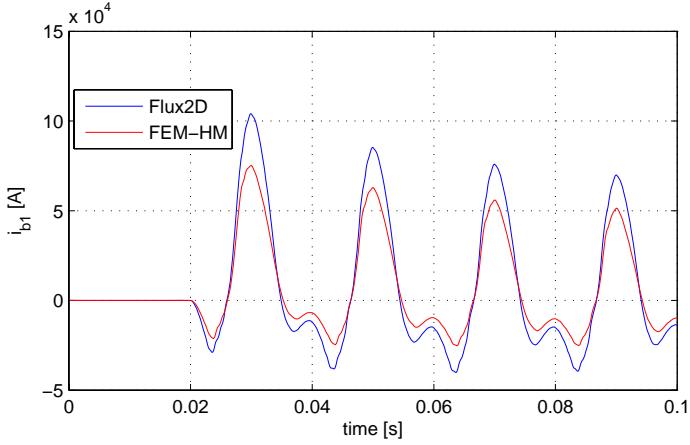**Fig. 8.10.** Current in the field winding.
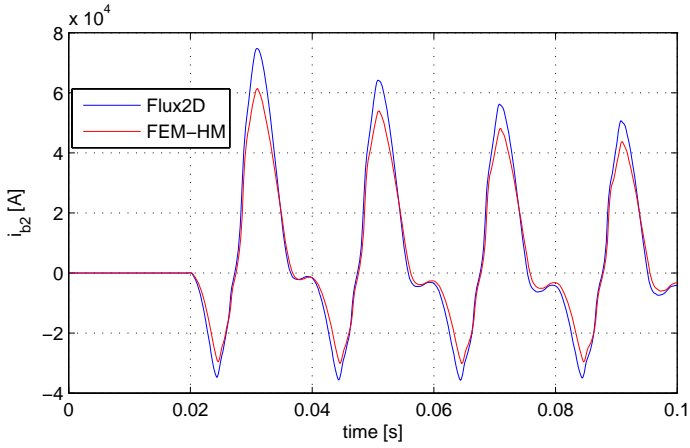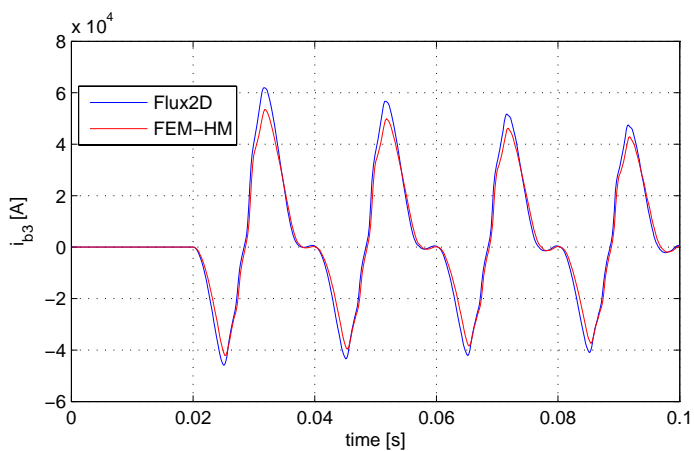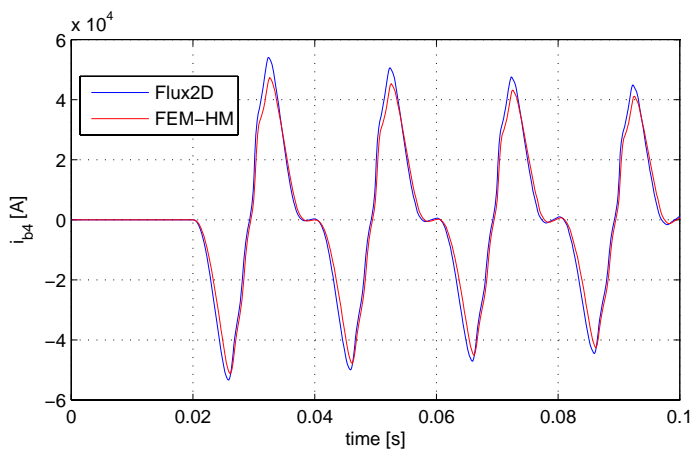
Fig. 8.11. Current in the 1st bar.

Fig. 8.12. Current in the 2nd bar.

Fig. 8.13. Current in the 3rd bar.

Fig. 8.14. Current in the 4th bar.
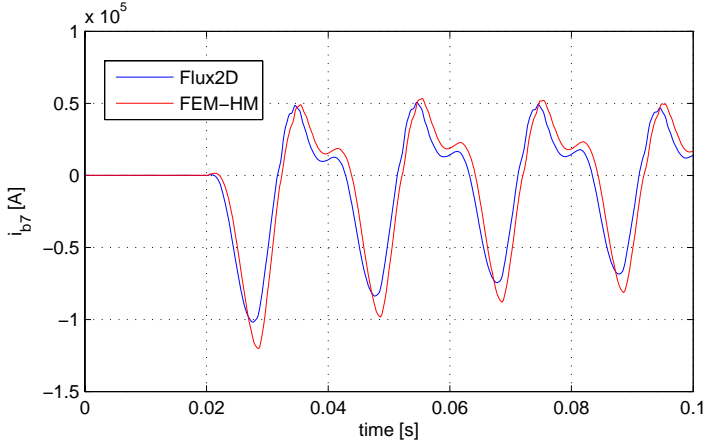
Fig. 8.15. Current in the 5th bar.
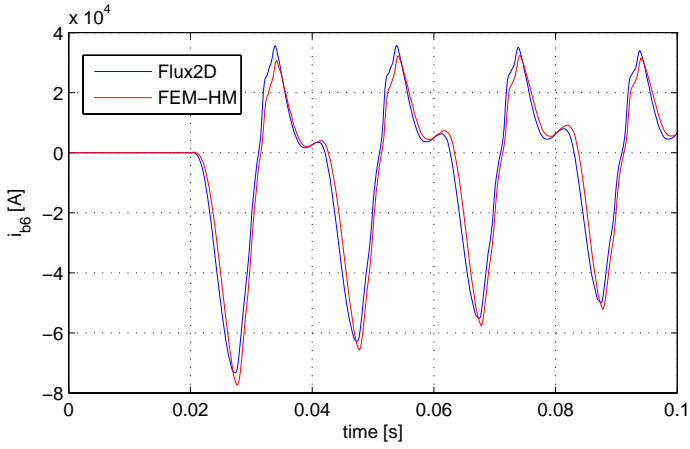
Fig. 8.16. Current in the 6th bar.
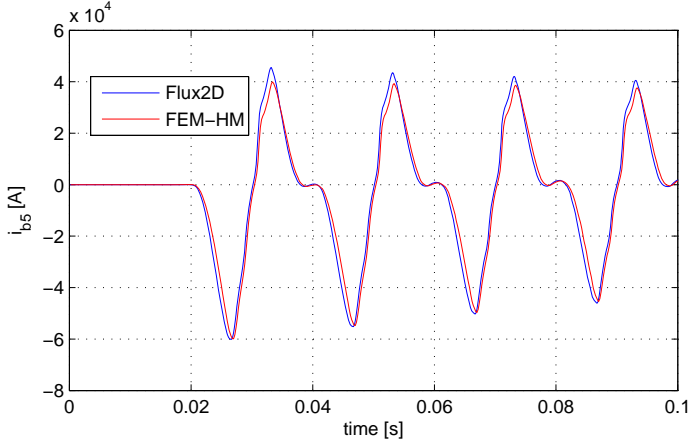
Fig. 8.17. Current in the 7th bar.

Torque

The torque computed by FEM-HM and Flux2D are compared in (fig. 8.18). The curve computed by FEM-HM closely follows the one issued from Flux2D. A shift between the two curves induces a rather large maximum error, 31%. The maximal value of both curves is nevertheless very similar.

8.6 Conclusion

This chapter presented the modelisation of a hydro generator with a complete damper cage. The geometry of the machine has been reduced to a single pole, by the use of anti-periodic boundary conditions. The modification to the circuit of the damper cage mandated by the anti-periodic boundary condition has been described.

Two simulations have been carried out. The first one was a computation of the induced voltage under no-load conditions. The values
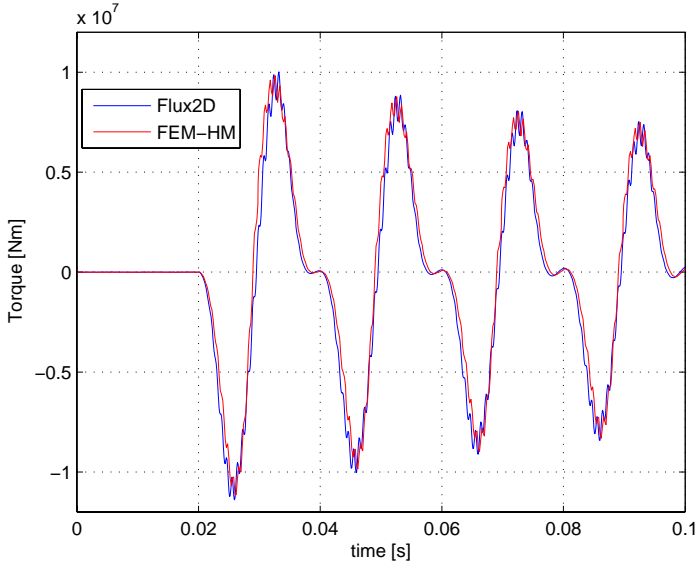
Fig. 8.18. Torque.

computed by FEM-HM are virtually identical to the one obtained with Flux2D. The second one is a two-phases short-circuit. Comparisons were made on the currents in the bars and the windings as well as on the torque.

The computations of the currents in the windings have been satisfactory. The curves of the field winding current computed by Flux2D and FEM-HM are virtually superposed. The curves of the stator windings currents computed by FEM-HM closely follow the ones from Flux2D.

The overall shape of the curves of the bars currents is correct. There is still however a discrepancy in their maximum values. This discrepancy can be explained by the different mesh used with FEM-

HM (fig. 8.19(a)) and Flux2D (fig. 8.19(b)). The mesh (fig. 8.19(a))
is clearly not of good quality in the sense of (sect. 2.2.2), as the
elements are needle shaped and there is a single layer of element
through the depth of the bars. The discrepancy is further exacer-
bated by the fact that Flu2D uses second degree form functions and
FEM-HM linear ones.

(a) FEM-HM.   (b) Flux2D.
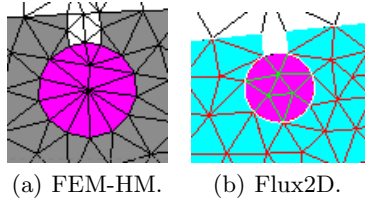
Fig. 8.19. Mesh in the bars.

The curve of the torque computed by FEM-HM closely follows
the one computed with Flux2D. The maximum values of both curves
are also close to each other, while they are shifted in time.

Even if the error on the bars current must still be reduced, it is
nevertheless possible to conclude that the circuit for the damper cage
reduced by anti-periodic limit conditions is implemented correctly.

9
Conclusion

The goal of this work was to add a FE model of the hydro generator to a grid simulation software. This has been divided into two sub-tasks. The first one is to create a program designed specifically for the simulation of hydro generator. The second is the creation of a link between said program and a grid solver.

9.1 FE program

The necessary features of the FE program have been described in (ch. 2). They are repeated here for convenience:

- ability to deal with non-linear materials;
- ability to take eddy currents into account;
- slide-band;
- simulation of a fraction of the machine through the use of periodic or anti-periodic boundary conditions;
- linkable with a grid simulation software.

Each of these features has been tested individually in simulations described in (ch. 4) to (ch. 6). In order to validate them, the same

simulations were also carried out with Flux2D. The comparisons of the results are conclusive.

First the non-linear solver needed to take the magnetic saturation into account has been tested on the single-phase transformer (sect. 4.1). Two switch-on from null initial conditions with different feed voltages were tried. The first one resulted in a short transient during which the currents never exceeded their steady-state values. The second one resulted in a much longer transient, with currents spiking to up to 10 times their steady-state values. Because of these currents, the yoke was highly saturated. Both of these cases were successfully simulated.

Then the prediction of eddy currents has been checked in (sect. 4.2). The geometry used is similar to the one of the single-phase transformer. However a third winding was added which was made of a single turn of massive conductor. The same switch-on as for the previous transformer was tried. For both of these cases the total current as well as the current density are accurately predicted by FEM-HM.

After that, the simulation of an unloaded three-phases transformer was carried out (ch. 5). This was used to validate the implementation of a three-phases circuit. This transformer, fed first by sinusoidal voltages then by square waves was successfully simulated.

Finally, the optimal re-meshing of the air-gap and the periodic boundary conditions were tested jointly by the simulation of a simple synchronous machine (ch. 6). The induced voltages computed with Flux2D and FEM-HM are virtually identical.

9.2 Linking method

Two linking methods, differential inductances and Newton-Raphson, have been described in (sect. 3.7). Both of them were tested on the admittedly simple simulation of the single-phase transformer (ch. 4) with accurate results. The Newton-Raphson method, being better suited to the task at hand (sect. 4.3.1), was chosen for this work.

Its stability was further checked on the example of the three-phases transformer (ch. 5). During these investigations no stability problems were encountered.

9.3 Simulations of rotating machines

The simulations of rotating machines are described in (ch. 7) for an induction machine and in (ch. 8) for a hydro generator. These two examples make use of all (but the periodic boundary condition in the case of the induction machine) the required features listed above.

Once again, the results obtained with FEM-HM linked to a Runge-Kutta routine simulating the feed circuit have been satisfactorily compared to Flux2D.

9.4 Conclusive remarks

Overall, the goals set for this work have been met: A FE program corresponding to the requirements has been written and a linking method between said program and a grid solver has been designed and validated.

Two tasks remain: First the link has been set up between FEM-HM and a simple Runge-Kutta 4 routine, not an actual grid solver. The work to link FEM-HM and SIMSEN is, at the time of writing, under way. Then FEM-HM is still in an experimental state. The results it delivers are accurate, however its user interface is not refined enough for general use.

A last comment about the computation speed. FEM-HM linked to a Runge-Kutta routine is about 15 time slower than Flux2D. Without link it is still 3 to 4 time slower. Speeding the computations is clearly also needed before FEM-HM can be used for industrial work.

References

[1] K. Hameyer, J. Driesen, H. De Gersem, and R. Belmans, "The classification of coupled field problems," *Magnetics, IEEE Transactions on*, vol. 35, pp. 1618 –1621, may. 1999.

[2] S. Dallas, J. Kappatou, and A. Safacas, "Investigation of transient phenomena of a salient pole synchronous machine during field short-circuit using fem," pp. 263 –268, jun. 2010.

[3] H. Lai, P. Leonard, D. Rodger, N. Allen, and P. Sangha, "3d finite element dynamic simulation of electrical machines coupled to external circuits," *Magnetics, IEEE Transactions on*, vol. 33, pp. 2010 –2013, mar. 1997.

[4] P. Lombard and G. Meunier, "A general method for electric and magnetic coupled problem in 2d and magnetodynamic domain," *Magnetics, IEEE Transactions on*, vol. 28, pp. 1291 –1294, mar. 1992.

[5] E. Melgoza, J. Guardado, V. Venegas, and J. Tovar, "Computation of the differential inductance matrix of magnetic devices by a sensitivity approach," in *11th International IGTE Symposium 2004*, pp. 157 – 160, 2004.

[6] E. Lange, F. Henrotte, and K. Hameyer, "An efficient field-circuit coupling based on a temporary linearization of fe electri-

cal machine models," *Magnetics, IEEE Transactions on*, vol. 45, pp. 1258 –1261, mar. 2009.

 [7] W. Vetter and K. Reichert, "Determination of damper winding and rotor iron currents in convertor- and line-fed synchronous machines," *Energy Conversion, IEEE Transactions on*, vol. 9, pp. 709 –716, dec. 1994.

 [8] S. Kanerva, S. Seman, and A. Arkkio, "Inductance model for coupling finite element analysis with circuit simulation," *Magnetics, IEEE Transactions on*, vol. 41, pp. 1620 – 1623, may. 2005.

 [9] A. Darabi and C. Tindall, "Damper cages in genset alternators: Fe simulation and measurement," *Energy Conversion, IEEE Transactions on*, vol. 19, pp. 73 – 80, mar. 2004.

[10] S. Kanerva, J. Kaukonen, A. Szucs, and T. Hautamaki, "Coupled fem-control simulation in the analysis of electrical machines and converters," pp. 1925 –1930, aug. 2006.

[11] M. Debarnot, P. Girard, M. Vilcot, U. Knorr, and L. Zacharias, "On line coupling of finite element analysis and system simulation for direct modelling of the complete controlled electromechanical chain without any equivalent diagram," Electrical Machines and Drives, 2000. International Conference on, aug. 2000.

[12] S. Seman, J. Niiranen, S. Kanerva, A. Arkkio, and J. Saitz, "Performance study of a doubly fed wind-power induction generator under network disturbances," *Energy Conversion, IEEE Transactions on*, vol. 21, pp. 883 –890, dec. 2006.

[13] W. Zhao, M. Cheng, W. Hua, and H. Jia, "Modeling of flux-switching permanent magnet motor drives using transient field-circuit co-simulation method," pp. 4044 –4048, oct. 2008.

[14] S. Ho, W. Fu, H. Li, H. Wong, and H. Tan, "Performance analysis of brushless dc motors including features of the control loop in the finite element modeling," *Magnetics, IEEE Transactions on*, vol. 37, pp. 3370 –3374, sep. 2001.

[15] M. Cervera, R. Codina, and M. Galindo, "On the computational efficiency and implementation of block-iterative algo-

rithms for nonlinear coupled problems," *Engineering Computations*, vol. 13, no. 6, pp. 4 – 30, 1996.

[16] G. Rosselet, M. TuXuan, and J.-J. Simond, "Using the newton-secant method for linking circuit-electromagnetic coupled simulation," *Magnetics, IEEE Transactions on*, to be submitted.

[17] "System simulation software for multi-domain design - Simplorer." Availlable:`http://www.ansoft.com/products/em/simplorer/`.

[18] G. Arians, T. Bauer, C. Kaehler, W. Mai, C. Monzel, D. van Riesen, and C. Schlensok, "Innovative modern object-oriented solving environment - iMOOSE." Available:`http://imoose.sourceforge.net`. [Online].

[19] "Maxwell." Availlable:`http://www.ansoft.com/products/em/maxwell/`.

[20] "Portunus." Availlable:`http://www.cedrat.com/index.php?id=39\&L=1\&no_cache=1`.

[21] A. Sapin, *Logiciel modulaire pour la simulation et l'étude des systèmes d'entraînement et des réseaux électriques 1346.* PhD thesis, EPFL, 1995.

[22] B. Kawkabani, G. Rosselet, and J.-J. Simond, "Combined analytical-numerical approach for the modeling and analysis of three-phase transformers," pp. 1521 –1526, nov. 2006.

[23] C. Ramirez, *Plateforme numérique d'essais 2821.* PhD thesis, EPFL, 2003.

[24] K. Hameyer and R. Belmans, *Numerical modelling and design of electrical machines and devices*, vol. 1 of *Advances in electrical and electronic engineering.* 1999.

[25] A. Abdel-Razek, J. Coulomb, M. Feliachi, and J. Sabonnadiere, "The calculation of electromagnetic torque in saturated electric machines within combined numerical and analytical solutions of the field equations," *Magnetics, IEEE Transactions on*, vol. 17, pp. 3250 – 3252, nov 1981.

[26] Cedrat, "Flux2d." `http://www.cedrat.com/en/software-solutions/flux.html`.

[27] D. Research, "Mtxvec." `http://www.dewresearch.com/mtxvec2.html`.

[28] "Linear algebra package." `http://www.netlib.org/lapack/`, May 2010.

[29] U. of Florida, "Unsymetric multifrontal package." `http://www.cise.ufl.edu/research/sparse/umfpack/`.

[30] J. A. Bastos and N. Sadowski, *Electromagnatic modeling by finite elemen method.* Marcel Dekker, 2003.

[31] P. Thomas, *Eléments finis pour l'ingénieur, grands principes et petites recettes.* EDF R&D, 2006.

[32] F. Gardiol, *Electromagnétisme*, vol. 3 of *Traité d'électricité.* Presses polytechniques et universitaires romandes, 1996.

[33] R. P. Feynman, R. B. Leighton, and M. Sands, *The Feynman lectures on physics*, vol. 2. Addison Wesley, 2006.

[34] E. Melgoza, J. L. Guardado, and V. Venegas, "A method for coupling electromagnetic transients programs with finite element magnetic field solvers," in *International Conference on Power System Transients (IPST'05)*, 2005.

[35] J. Chatelain, *Machines électriques*, vol. 10 of *Traité d'électricité.* Presses polytechniques et universitaires romandes, 1989.

[36] M. Jufer, *Electromécanique*, vol. 9 of *Traité d'électricité.* Presse polytechniques et universitaires romandes, 1995.

[37] M. Moallem and C.-M. Ong, "Predicting the torque of a switched reluctance machine from its finite element field solution," *Energy Conversion, IEEE Transactions on*, vol. 5, pp. 733–739, Dec 1990.

[38] P. P. Silvester and R. L. Ferrari, *Finite elements for electrical engineers.* Cambridge University Press, 1996.

[39] Cedrat, "Flux2d 7.60 application induction motor technical paper."

[40] R. Boite and J. Neirynck, *Théorie des réseaux de Kirchhoff*, vol. 4 of *Traité d'électricité.* Presses polytechniques et universitaires romandes, 1996.

Curriculum vitae

Gilles Rosselet   Born 10th January 1979, single

Studies

2010	Research assistant
	LME, EPFL, Lausanne Switzerland
2004	Ms Ing
	Section for electrical and electronic ing.
	EPFL, Lausanne, Switzerland
1997	High school diploma, scientific
	Lycée Denis de Rougemont,
	Neuchâtel Switzerland

Languages

French	motherlanguage
English	good written and spoken skills
German	school knowledge

Publication

Kawkabani, B.; Rosselet, G. and Simond, J.-J.; "Combined Analytical-Numerical Approach for the Modelling and Analysis of Three-phase Transformers", *Annual Conference of the IEEE Industrial Electronics Society* 2006, Paris, France.

Rosselet, G.; TuXuan M. and Simond J.-J.; "Using the Newton-Secant Method for linking Circuit-Electromagnetic coupled simulation", *Magnetics, IEEE Transactions on*, to be submitted.